Chemical Engineering Science 254 (2022) 117612

Contents lists available at ScienceDirect

Chemical Engineering Science

journal homepage: www.elsevier.com/locate/ces

Geometric and thermodynamic considerations of saturated and slightly subcooled water flow through nozzles

Gregory G. Hendrickson [a,*], Daniel K. Smith [b], Robert N. D'Alessandro [c], Georges A. Melhem [d], Marc E. Levin [e], Harold G. Fisher [f], Leonid Korelstein [g]

[a] Retired, 2018 Lazy Grove Drive, Kingwood, TX 77339, USA
[b] Albemarle Corporation, Gulf States Road, Baton Rouge, LA 70805, USA
[c] Retired, Spanish Fort, AL 36527, USA
[d] ioMosaic Corporation, 93 Stiles Road, Salem, NH 03079, USA
[e] Independent Consultant, Spokane, WA 99223, USA
[f] Fisher Inc., 229 Brookhaven Drive, Nitro, WV 25143, USA
[g] Piping Systems Research & Engineering Company (NTP Truboprovod), Plehanova str., 7, Moscow 111141, Russia

HIGHLIGHTS

- Deviation from equilibrium is recognized as a manifestation of rapid depressurization events including Rapid Phase Transitions, Boiling Liquid Expanding Vapor Explosions, and flow of saturated and slightly subcooled liquids through converging nozzles and sudden contractions.
- Non-equilibrium effects are attributed to nozzle geometry and the pressure driving force for saturated and slightly subcooled liquid flow through nozzles and sudden contractions.
- Bubble nucleation theory is used to estimate the deviation from equilibrium and single-phase flow methods are used to estimate the critical mass flux when rapid vaporization occurs at the nozzle throat.

ARTICLE INFO

Article history:
Received 2 December 2021
Received in revised form 9 March 2022
Accepted 11 March 2022
Available online 17 March 2022

Keywords:
Choked flow
Non-equilibrium
Bubble nucleation
Superheating
Rapid depressurization
Metastability

ABSTRACT

It is well known that homogeneous equilibrium methods for calculating the mass flux of initially subcooled or saturated liquids in short nozzles under-predict the measured values and various methods for estimating non-equilibrium effects have been presented in the past. It is shown in this paper that acceleration effects at the entrance of converging nozzles due to changing cross-sectional area and approach to thermodynamic saturation pressure at the point of maximum fluid acceleration can be the most significant causes of non-equilibrium. By properly accounting for non-equilibrium due to the fluid acceleration, single-phase flow methods can be used to estimate the pressure loss and mass flux in nozzles when rapid vaporization occurs at the nozzle throat. For these cases, choking occurs due to the rapid vaporization while the difference between the inlet pressure and choking pressure determines the nozzle mass flux.

1. Introduction

Thermal non-equilibrium phenomena have been recognized in the critical flow of fluids through short pipes and nozzles for several decades. According to Weisman and Tentner (1978), early studies of non-equilibrium include the works of Benjamin and Miller (1942), Burnell (1947), Hodkinson (1937) and Silver and Mitchell (1945). It is clear that there are at least two mechanisms of thermal non-equilibrium in subcooled/saturated/low-quality flow:

- Non-equilibrium vaporization (maybe after some delay of vaporization) for some relaxation period of time characteristic of low inlet quality flow.
- Delay of nucleation (with metastable liquid) characteristic of subcooled/saturated inlet flow.

Various Homogeneous Non-Equilibrium (HNE) models and a Delayed Equilibrium Model (DEM) have been developed to account

* Corresponding author.
E-mail address: greghendrickson1954@gmail.com (G.G. Hendrickson).

https://doi.org/10.1016/j.ces.2022.117612
0009-2509/

Nomenclature

A	flow area
C	Burnell (1947) factor (Equation (4.6))
C_D	discharge coefficient
d	inside diameter
d_c	diameter in the nozzle converging portion
D	large diameter
f_D	Darcy (Moody) friction factor
g_c	Newton's law conversion factor
G	mass flux
G_c	critical mass flux
h	vertical displacement
h_0	(D-d)/2
k	Boltzmann's constant
l	length of nozzle constant-diameter portion
L	length of Sozzi and Sutherland nozzle converging section
$\dot{m}$	mass flow rate
N	HNE model non-equilibrium parameter
P	pressure
P_0	nozzle inlet pressure
$P_{a,max}$	pressure at the point of maximum depressurization rate
P_{Fi}	flashing inception pressure
P_n	bubble nucleation pressure
$P_{n,A-L}$	bubble nucleation pressure calculated using the Alamgir and Leinhard correlation
$P_{n,relaxed}$	bubble nucleation pressure calculated using approach to equilibrium efficiency
P_o	stagnation pressure
P_s	fluid saturation pressure
P_t	nozzle throat pressure (e.g., exit of the straight section)
P_u	fluid undershoot pressure
t	time
T	temperature
T_c	thermodynamic critical temperature
T_i	inlet (initial) temperature
T_r	reduced temperature (T/T_c)
u	velocity
v	specific volume
v_f	fluid specific volume
v_g	gas specific volume
x	fluid quality
x_E	equilibrium fluid quality
x_0	inlet quality
z	axial distance
$z_{a,max}$	location of maximum depressurization rate
η	efficiency
θ	relaxation time
ρ	density
ρ_t	fluid density at the nozzle throat
ρ_0	fluid density at the nozzle inlet
σ	surface tension
Σ'	depressurization rate
Σ'_0	transient depressurization rate equal to zero for steady flows
τ	residence time
ϕ	bubble nucleation heterogeneity factor

for non-equilibrium vaporization in critical flow through nozzles. A characteristic of the HNE models is the introduction of an empirical non-equilibrium parameter, "N", to represent deviation from equilibrium, equation (1.1).

$$\frac{dx}{dP} = N\frac{dx_E}{dP} \tag{1.1}$$

The non-equilibrium parameter was introduced by Henry (1968, 1970) and modified by Henry and Fauske (1971). More recent modifications of the HNE method include the HNE-DS by Diener and Schmidt (2004, 2005) and Schmidt (2007) and the ω-HNE by Leung (2013, 2019). The cited literature indicates the non-equilibrium parameter is dependent upon the flowing fluid's physical and thermodynamic properties and the flow path geometry. In a related approach proposed by Yoon, et.al (2006), the non-equilibrium parameter is an exponential function of the fluid relaxation time.

Critical flow through nozzles described by the DEM consists of three phases – saturated vapor, saturated liquid and metastable liquid (De Lorenzo, 2018). The metastable liquid is formed upon rapid depressurization of an initially subcooled or saturated liquid. The saturated vapor and liquid are formed upon relaxation of the metastable liquid and are assumed to be in equilibrium. The metastable fluid relaxation rate is described by a relaxation law. The onset of nucleation is specified in the DEM to occur at 0.95 times the saturation pressure (Bartosiewicz, et.al, 2011) to 0.975 times the saturation pressure (Seynhaeve, et.al, 2015).

The non-equilibrium phenomena addressed in this paper are the delay of nucleation and rapid phase transition associated with the rapid depressurization of initially slightly subcooled or saturated liquids. The onset of nucleation occurs at a pressure determined by the amount of initial subcooling and the depressurization rate. A rapid phase transition, coincident with choking, occurs essentially only at the nozzle throat.

2. Rapid phase Transitions

When initially subcooled or saturated liquids are subjected to rapid pressure reduction below the liquid saturation pressure without bubble nucleation, the fluid is said to be superheated. The superheated state is thermodynamically metastable and typically the fluid begins to vaporize after a delay time which depends on the bubble nucleation rate. These concepts are illustrated in Fig. 2.1 for nozzle flow. The fluid pressure drops rapidly below the fluid saturation pressure in the nozzle converging section. Vaporization starts after the nucleation delay time represented by the "Boiling Delay" line. After sufficient residence time the fluid pressure approaches the saturation pressure because of fluid relaxation phenomena, represented by the "Equilibrium" line. In short nozzles, choking can occur at the nozzle throat before equilibrium is established. In this case, the nozzle throat pressure is below the fluid saturation pressure and consequently the actual flow rate established is greater than that predicted by models incorporating the assumption that equilibrium occurs.

The bubble nucleation rate depends on the amount of superheating as described by bubble nucleation kinetic theory (Brennen, 1995). Correspondingly the amount of superheating is limited by thermodynamics. Thermodynamic stability analysis indicates phase change occurs spontaneously at the spinodal temperature (Lienhard et al., 1986). Therefore, when a fluid is highly superheated, the vaporization commences and proceeds at a rapid rate. The process of rapid phase transition is called explosive boiling. The same bubble nucleation kinetic and thermodynamic

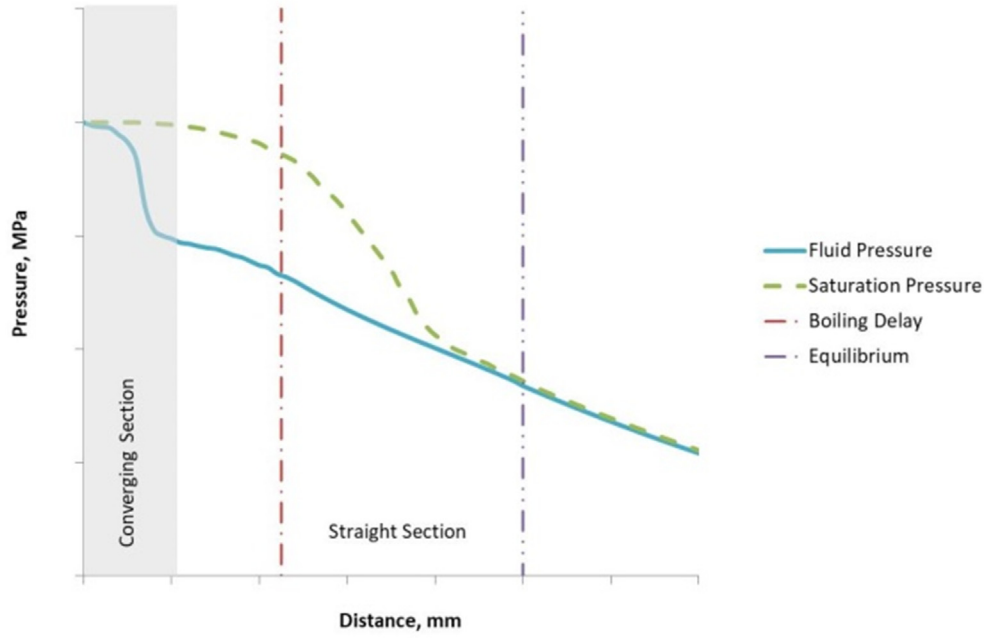

Fig. 2.1. Representative Nozzle Pressure Profile.

stability analyses apply to various phenomena including Rapid Phase Transitions (RPT), Boiling Liquid Expanding Vapor Explosions (BLEVE) and flow through nozzles. Examples of RPT applications are found in Melhem and Hendrickson (2020) while BLEVE applications are found in Mengmeng (2007). The focus of this paper is the application of bubble nucleation kinetics and thermodynamic stability analyses to the flow of subcooled and saturated liquids through nozzles. The proposed method addresses known deficiencies of the Homogeneous Equilibrium Model (HEM) by providing a method to quantify non-equilibrium effects on calculated nozzle choking pressures and critical mass flow rates.

3. Why subcooled flow estimates matter

Numerous plant design and hydraulic applications, including pressure relief systems, require reasonable flow rate estimates of initially saturated or slightly subcooled liquids. Current equilibrium based methods, such as the HEM, underestimate the flow rate depending on the degree of liquid subcooling.

Underestimating the actual flow rate in process safety does not necessarily result in a safe design. For example, flow rates predicted using the HEM can result in underestimating leak rates for dispersion modeling or under predicting the rate of material transfer during a process upset. Also, the selection of suitably sized relief devices using the HEM can result in significantly oversized pressure relief devices in some situations. While these oversized devices do result in adequate pressure protection for the process equipment, the downstream equipment for separation, flaring and/or vent containment can receive much higher flow rates than premised in the design. Oversizing the pressure relief devices can be costly and not knowing the flow rate accurately can be detrimental to the performance of downstream safety systems.

On the other hand, proper accounting of non-equilibrium flow phenomena offers a potential opportunity to save capital investments during pressure relief device revalidation projects. "Capacity creep" and debottlenecking projects in refineries and chemical plants can increase the required overpressure relief flow rate. It is not uncommon for the increased required flow rate to exceed the calculated capacity of installed pressure relief devices when equilibrium flow is assumed. It is foreseeable that accounting for the increased flow due to non-equilibrium effects can address seeming capacity deficiencies that would otherwise require modifications in the field (e.g., installing larger pressure relief devices).

In the nuclear industry, flow of reactor coolant during a Loss of Coolant Accident (LOCA) is characterized by non-equilibrium flow through a break in one of the coolant pipes. It is critical to estimate the coolant flow rate through a leak during a LOCA in order to design the emergency coolant systems to mitigate the consequences of the scenario.

4. Background

The fundamental equation for the determination of mass flux through a relief valve nozzle is the differential form of the steady-state, constant elevation and frictionless Bernoulli equation

$$udu = -vdP = -\frac{dP}{\rho} \tag{4.1}$$

Note: Variables are defined in the Nomenclature section. Integration from the stagnation state $(P = P_0, u = 0)$ to the nozzle throat (e.g., exit) pressure and expressing the result in terms of the mass flux yields

$$G = \rho_t \left[-2 \int_{P_0}^{P_t} \frac{dP}{\rho} \right]^{1/2} \tag{4.2}$$

Note this equation makes no provision for the geometry of the nozzle. This result becomes the Homogeneous Equilibrium Model (HEM) for nozzles when the flow is vapor–liquid two-phase flow and the following are assumed:

- The pressures in both phases are equal
- The temperatures in both phases are equal (thermal equilibrium)
- The velocities of both phases are equal (mechanical equilibrium)
- The Gibbs free energies (chemical potentials) of both phases are equal (chemical equilibrium)

- Homogeneity (the fluid is modeled as a single phase with thermodynamic properties that are the average of the two phases)

When a subcooled or saturated liquid flow is analyzed using the HEM, pressure reduction along an isentropic flow path is nearly isothermal for small degrees of subcooling. However, the temperature increases slightly if the initial subcooling is achieved by increasing the pressure at constant entropy. Thus, as the initial pressure increases, depressurization along an isentropic flow path can result in some amount of temperature reduction with the amount of temperature reduction increasing as the initial pressure increases. In either case, the critical mass flux from application of Equation (4.2) with the homogeneous equilibrium assumptions often occurs when the nozzle throat pressure is near the fluid saturation pressure. Isothermal depressurization from point A to point B located at the fluid saturation pressure is illustrated in Fig. 4.1. The square at the top of the two-phase region represents the critical point.

When the fluid remains a saturated liquid for the majority of the flow path and the nozzle throat pressure is approximately equal to the fluid saturation pressure, a close estimate of the HEM flux can be obtained using the Bernoulli equation with the throat pressure equal to the saturation pressure.

$$G = \sqrt{2\rho_0(P_0 - P_s)} \tag{4.3}$$

See for example Leung and Ciolek (1994) who state that the use of the saturation pressure in the Bernoulli equation is appropriate due to choking at the throat for longer flow lengths (L/D = 25, 50 and 100) when the HEM assumptions are appropriate. When frictional effects are included with constant elevation and thermodynamic equilibrium, the integrated Bernoulli equation becomes

$$G = \sqrt{\frac{2\rho_0(P_0 - P_s)}{1 + f_D \frac{l}{d}}} \tag{4.4}$$

In contrast, when non-equilibrium effects are important, the Bernoulli equation approximation to the HEM (Equations 4.3 or 4.4) under-predicts the critical mass flux for slightly subcooled and saturated liquid inlet conditions. It has long been known that the HEM under-predicts the mass flux for nozzle flow with inlet conditions near the fluid saturation conditions. Early literature reviews presented by Saha (1978) and by Hsu (1972) indicate the HEM under-predicts critical discharge rates for short pipes and near saturation or subcooled upstream conditions due to the liquid superheat.

The critical mass fluxes calculated using Equation (4.4) are compared with measured mass flux data for saturated and subcooled water flow from Sozzi and Sutherland (1975) in Fig. 4.2. Inspection of Fig. 4.2 reveals that the error in the calculated mass flux increases as the fluid subcooling decreases and as the nozzle length decreases. This deviation has been attributed to non-equilibrium effects. Note: inclusion of frictional effects is important for longer nozzles. The calculated mass flux is higher than the measured mass flux for longer nozzles and large subcooling when friction is ignored.

Various approaches have been proposed to more accurately predict the critical nozzle flow of saturated and subcooled liquids. A method proposed by Burnell (1947) includes a correction factor, the Burnell C factor, in the Bernoulli equation.

$$G = \sqrt{2\rho_0[P_0 - (1 - C)P_s]} \tag{4.5}$$

To account for friction, the $f_D l/d$ term can be retained.

$$G = \sqrt{\frac{2\rho_0[P_0 - (1 - C)P_s]}{1 + f_D \frac{l}{d}}} \tag{4.6}$$

Examples from the literature for correlations of the Burnell C factor include Weisman and Tentner (1978), Sallet and Sommers (1985), and Kim (2015a). Weisman and Tentner (1978) show a correlation with the nozzle inlet saturation pressure for water flow (Fig. 4.3). Sallet and Sommers (1985) reported a correlation with nozzle inlet stagnation temperature developed by Burnell (1947) for water flow.

$$C = 0.264\left[\frac{75.48 - 0.14T}{49.2}\right] \text{where} T[=]^{\circ}C \tag{4.7}$$

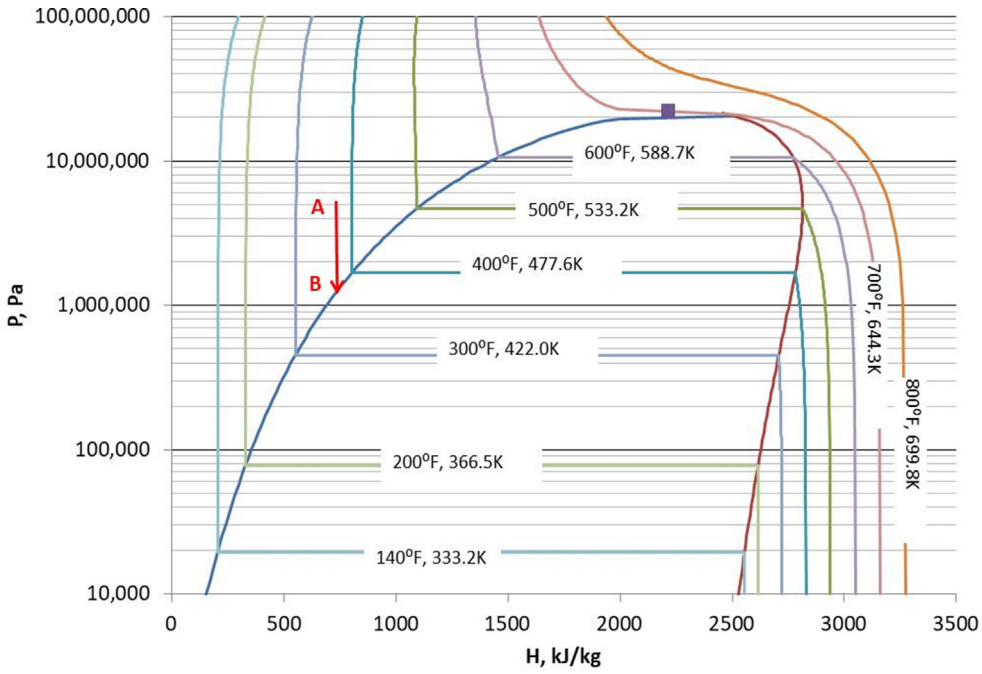

Fig. 4.1. Flashing Commences near the Saturation Curve.

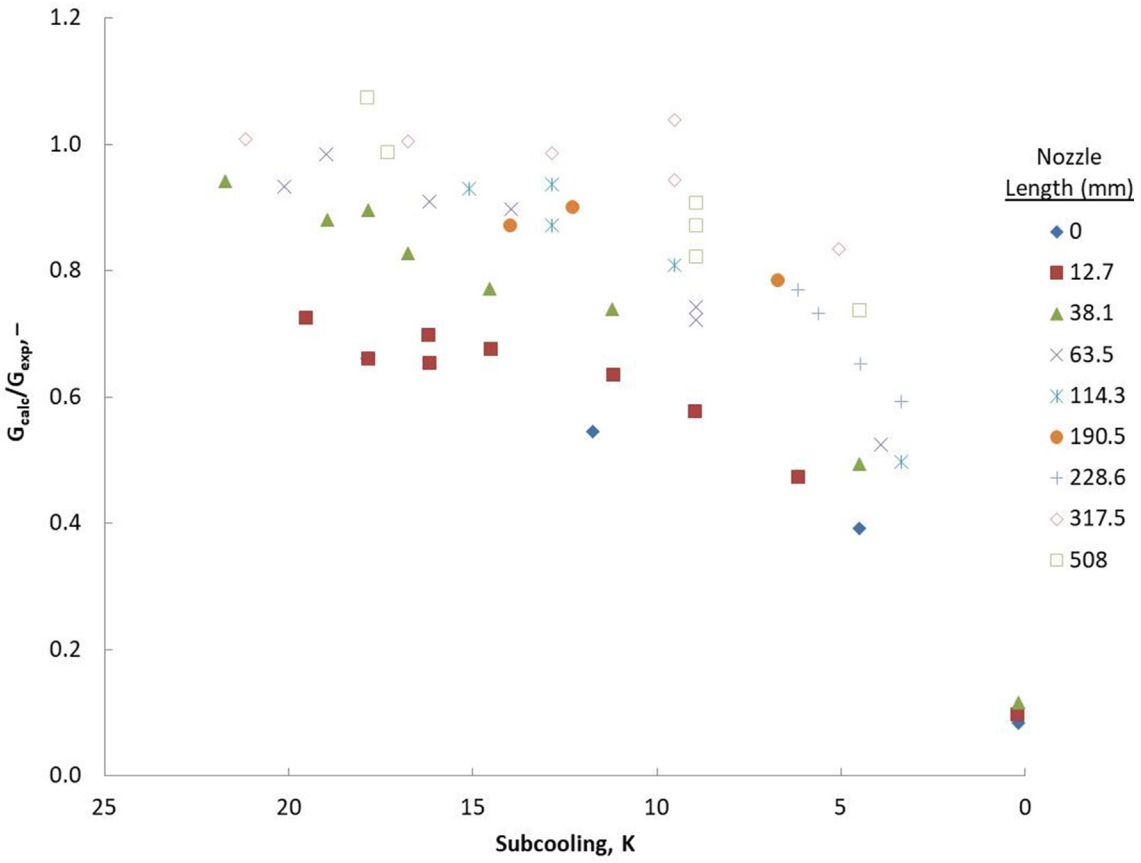

Fig. 4.2. Comparison of Bernoulli Equation Calculated Flow with Sozzi and Sutherland (1975) Data.

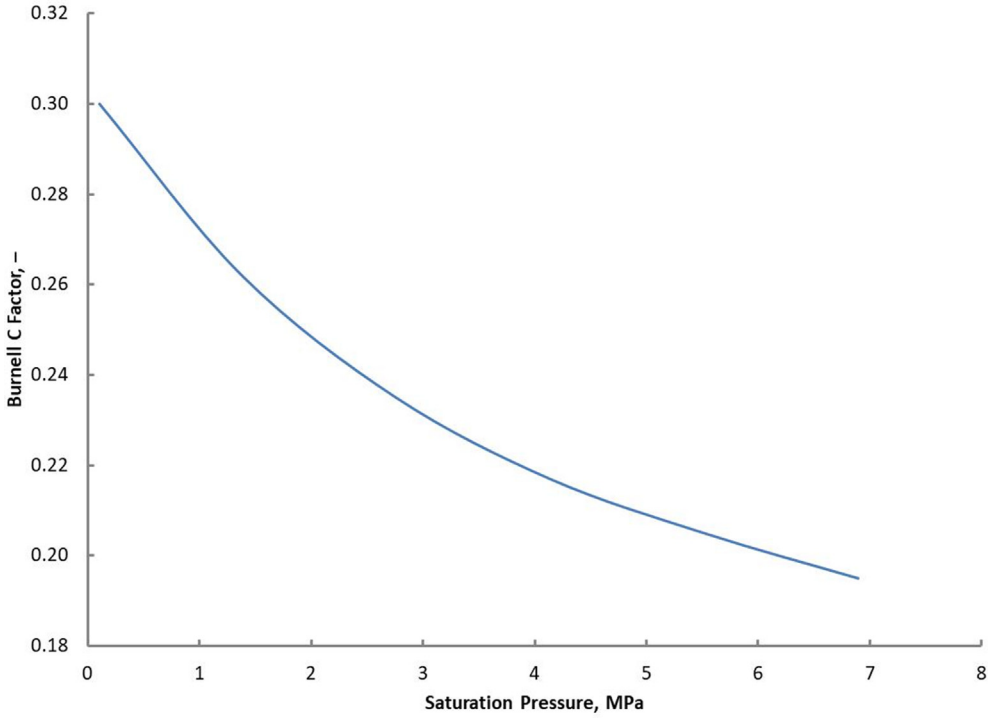

Fig. 4.3. Weisman and Tentner (1978) Correlation for Burnell C Factor.

Sallet and Sommers (1985) also reported that Equation (4.7) was derived using a surface tension versus temperature correlation.

In summary, the flow of saturated and slightly subcooled liquids in nozzles is characterized by a rapid pressure decrease to a non-equilibrium superheated state. The superheated liquid is referred to as a metastable fluid. Upon depressurization, flashing does not typically commence until the fluid pressure falls below the fluid saturation pressure. The amount of pressure-undershoot (or equivalently, the amount of fluid superheating) is determined by non-equilibrium phenomena. The Burnell method can be thought of as representing single-phase metastable fluid flow into the two-phase envelope until rapid vaporization occurs at the nozzle throat. The thermodynamic path of depressurization into the two-phase region is illustrated in Fig. 4.4. As the pressure is reduced from Point A to Point B a metastable fluid is formed when the fluid pressure decreases below the saturation pressure. Vaporization commences and choking occurs at Point B rather than at the saturation pressure. The square at the top of the two-phase envelope represents the critical point.

5. Non-equilibrium flow model description

A premise of the proposed calculation method is that when saturated and slightly subcooled liquids flow through converging nozzles, the observed non-equilibrium effects are a manifestation of the rapid depressurization upon acceleration of the fluid in the nozzle converging section. It has been demonstrated in bubble nucleation literature, see for example Alamgir and Lienhard (1981), that the amount of pressure-undershoot (e.g., superheating) depends on the rate of depressurization. The difference between the fluid saturation pressure and the bubble nucleation pressure increases as the depressurization rate increases. In nozzle flow the rate of depressurization is related to the rate of fluid acceleration and thus also to the geometry of the converging flow area. In other words, the amount of thermal non-equilibrium is determined by the nozzle geometry and rate of acceleration pressure decrease. When rapid vaporization occurs at the nozzle throat, the nozzle throat pressure can be represented by the bubble nucleation pressure. Further, Burnell's C factor can be correlated with the rate of depressurization due to the fluid acceleration into the nozzle.

The proposition is illustrated using a generic converging nozzle (Fig. 5.1) and described as follows. *Note the same principles also apply to square-edged inlets if acceleration into the vena contracta is properly modeled.* The fluid is accelerated in the converging section of the nozzle due to the pressure driving force. The rate of this acceleration pressure loss determines the amount of superheating, e.g., the undershoot pressure, as determined by the bubble nucleation pressure. For a given overall pressure drop, as the friction loss in the straight section of the nozzle increases, the amount of pressure drop available for acceleration loss in the converging section decreases, i.e., increasing the length of the straight section of the nozzle downstream of the converging section decreases the acceleration losses in the converging section. *Thus, the departure from equilibrium in the converging section decreases as the friction loss in the straight section increases.* This interpretation is consistent with the rule of thumb that equilibrium flow occurs when the nozzle length is greater than 100 mm (4 in.); namely, the length provides enough friction loss (e.g., back pressure) to cause the bubble nucleation pressure to approach the fluid vapor pressure in the converging section. Furthermore, for a range of nozzle lengths, the friction losses of the metastable fluid in the straight section of the nozzle can be represented by the single-phase Darcy–Weisbach equation (Equation (5.1)) and choking occurs due to rapid vaporization essentially at the nozzle throat. The Darcy–Weisbach equation can be used to compute pressure drop for laminar or turbulent flow using an empirical friction factor (Benedict, 1980).

$$\Delta P = f_D \frac{l}{d} \frac{\rho u^2}{2g_c} \tag{5.1}$$

This interpretation is consistent with observations that flashing primarily occurs near the location of minimum pressure (Shin and Jones, 1993), e.g., the nozzle throat.

The Bernoulli equation with the throat pressure equal to the saturation pressure (Equation (4.4)) can be used to estimate the

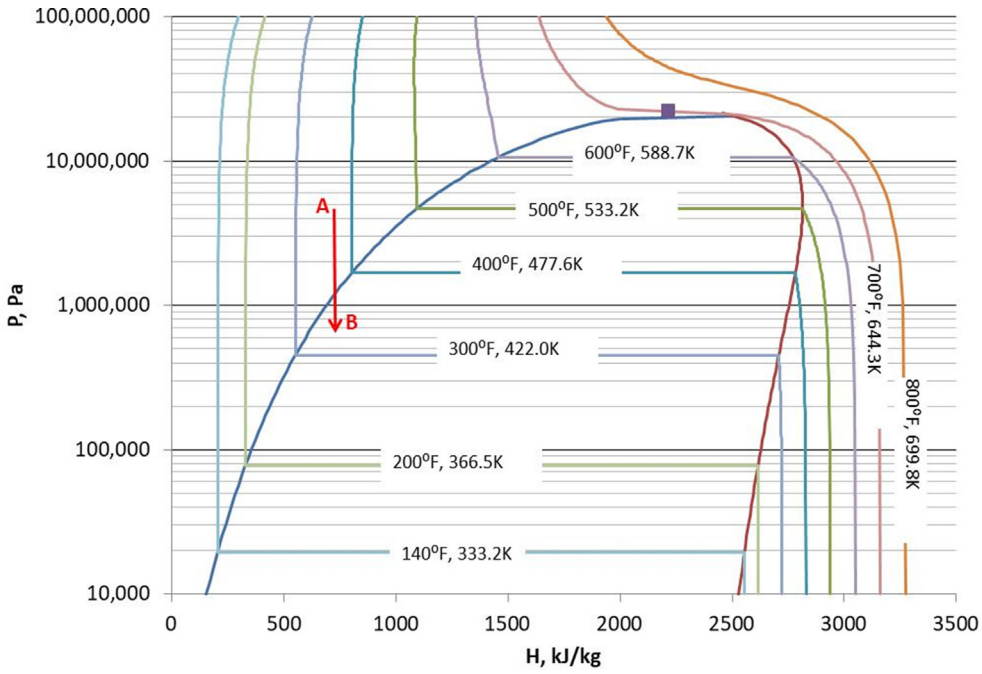

Fig. 4.4. Flashing Commences inside the Two-Phase Envelope.

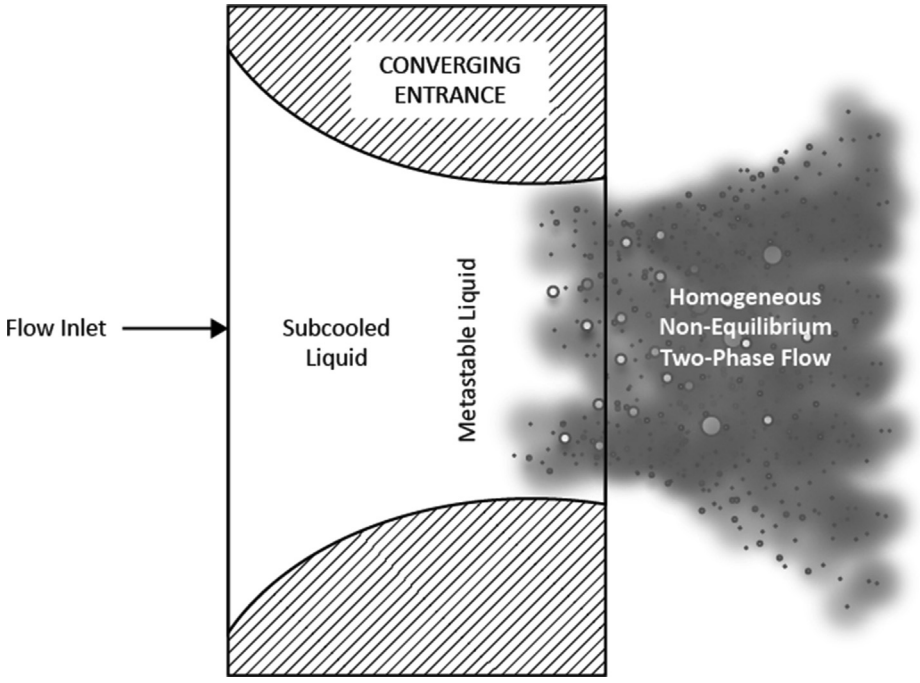

Fig. 5.1. Generic Converging Nozzle.

mass flux when single-phase flow occurs over most of the nozzle length and equilibrium flashing approximately coincident with choking occurs essentially only at the nozzle throat. This view of choking is commonly accepted for equilibrium flow of subcooled and saturated fluids. It will subsequently be shown that, by application of bubble nucleation dynamics to estimate the nozzle throat pressure, the Bernoulli equation with the throat pressure equal to the bubble nucleation pressure can be used to estimate the mass flux when single-phase flow occurs over most of the nozzle length and non-equilibrium flashing approximately coincident with choking occurs essentially only at the nozzle throat. *The difference between the flow of equilibrium fluids and metastable fluids in nozzles is that equilibrium fluids flash at the thermodynamic vapor pressure while metastable fluids flash at a pressure lower than the thermodynamic vapor pressure.*

6. Overview of bubble nucleation and growth

Vapor bubbles can only form if sufficient energy is available to overcome the cohesive forces of the liquid and create a void space for the vapor. Bubbles with sufficient energy to attain a critical size can survive and grow to larger sizes while bubbles with insufficient size collapse. Nucleation is the formation of the critically sized or larger bubbles. The radius of a spherical bubble of this sufficient size is known as the critical radius.

Fig. 6.1 illustrates the three phases of bubble growth in superheated liquids. Bubble nucleation commences after a finite delay time. Upon nucleation, the bubble radius is just larger than the critical radius. Initially surface tension impedes bubble growth. After the bubble grows somewhat (Miyatake et al. (1997) suggest doubling the diameter), inertia forces dominate and the bubble growth is primarily due to the difference in the pressure of the vapor inside the bubble and the fluid pressure exterior to the bubble. The pressure of the vapor inside the bubble is related to the local fluid thermodynamic vapor pressure by the Poynting correction factor. During this phase the bubble growth is approximately linear with respect to time. As the bubble grows further, its temperature drops causing a temperature difference between the surrounding fluid and bubble interior. In this phase the bubble growth rate is dominated by heat transfer from the surrounding liquid, which causes the addition of vapor to the bubble by evaporation at the vapor–liquid interface. During this phase the bubble growth is approximately proportional to the square root of time.

Common assumptions in equilibrium models of two-phase flow cannot account for bubble dynamics when the bubble nucleation delay time is significant compared to the fluid residence time in the nozzle and when significant pressure and temperature differences exist between the liquid and vapor phases. According to Yoon et al. (2006), thermal non-equilibrium has been shown to be related to bubble nucleation because several researchers used a nucleation delay time on the order of 1 ms in homogeneous non-equilibrium models to predict experimental results. Bubble nucleation delay is consistent with experimental results and provides an explanation for rapid phase transition phenomena. The challenge is to relate bubble nucleation phenomena to nozzle flow phenomena.

7. Metastable fluid formation and bubble nucleation in nozzle flow

The importance of non-equilibrium effects in nozzle flow has long been recognized. According to Angelo et al. (2012), the idea of a metastable fluid is not new; rather it was introduced by Silver and Mitchell (1951). Because the degree of superheat is directly related to the amount of pressure decrease below the saturation pressure, these concepts can be used interchangeably to describe deviation from equilibrium upon pressure reduction.

Credit has been given to Alamgir and Lienhard (1981) for first examining pressure-undershoot. They developed a semi-empirical correlation, motivated by classical nucleation theory, to predict the pressure-undershoot below the saturation pressure at the onset of flashing during the rapid depressurization of hot water. Alamgir and Lienhard developed the depressurization rate, Σ', dependent heterogeneity factor correlation given by Equation (7.1) and the pressure-undershoot correlation given by Equation

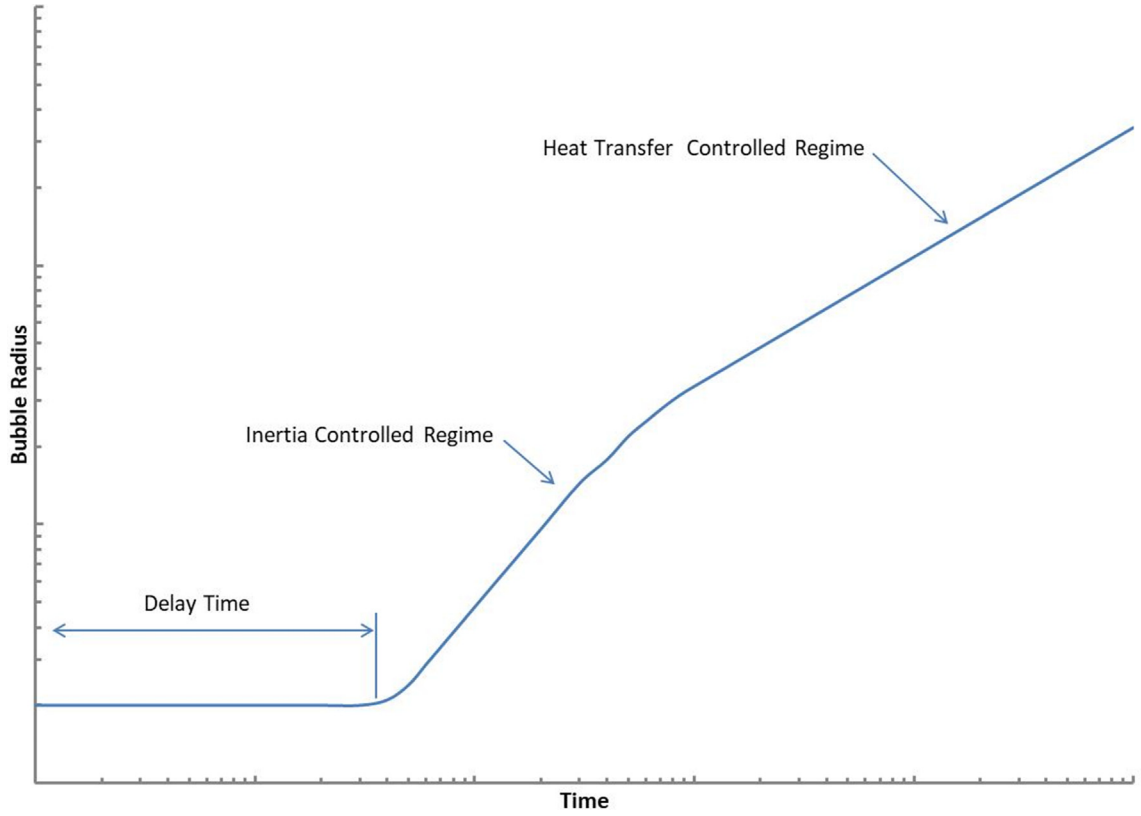

Fig. 6.1. Bubble Growth Development.

(7.2). For convenience, Equation (7.2) will be referred to as the "Alamgir and Lienhard correlation".

$$\varphi = 0.1058 T_r^{28.46}\left[1 + 14\left(\Sigma'\right)^{0.8}\right] \tag{7.1}$$

$$P_s(T_i) - P_n = 0.252\frac{\sigma^{3/2}T_r^{13.73}\left[1 + 14\left(\Sigma'\right)^{0.8}\right]^{1/2}}{\sqrt{kT_c}\left(1 - \frac{v_f}{v_g}\right)} \tag{7.2}$$

Note: Lienhard et al. (1986) provided a review of equations of state and the prediction of spinodal lines and incorrectly showed the quantity ($1\text{-}v_f/v_g$) under the square root sign (their Equation 28). The term should be outside the square root sign as shown in Equation (7.2). This correction is consistent with the original Alamgir and Lienhard (1981) correlation (their Equation 13). Also note the precise value of the constant in front of Equation (7.2) is 0.2507 rather than 0.252. When reference is made to the Alamgir and Lienhard correlation their value of 0.252 is retained.

The Alamgir and Lienhard correlation is dimensional, with depressurization rate units of Matm/s (Mega-atm/s). Surface tension, Boltzmann constant, temperature and pressure units are self-consistent. The correlation was developed for

$$0.62 \le T_r \le 0.935 and 0.004 \le \Sigma' \le 1.8 Matm/s (405 \le \Sigma' \le 182,000 MPa/s)$$

The model should not be used to accurately predict the nucleation pressure for smaller depressurization rates without changing the correlation constants.

Abuaf et al. (1983) stated that "according to accepted concepts" for nozzle flow with subcooled inlet conditions, the liquid accelerates in the converging section causing the local pressure to drop below the saturation pressure. The resulting metastable superheated fluid flow is essentially a single phase until it reaches the flashing inception point. Abuaf *et al.* utilized the correlation developed by Alamgir and Lienhard combined with a correlation for turbulence intensity to demonstrate the flashing inception point is essentially located at the plane of minimum cross-sectional area in converging–diverging nozzles.

With flashing inception at the nozzle throat, single-phase flow was considered upstream of the throat. For liquids with constant density, the critical mass flux was then given by

$$G_c = C_D\sqrt{2\rho(P_0 - P_s + \Delta P_{Fi})} \tag{7.3}$$

The pressure differential to flashing inception (ΔP_{Fi}) is obtained using the Alamgir and Lienhard correlation. Note the similarity between the Abuaf *et al.* equation and the Burnell equation. The pressure differential to flashing inception and the Burnell C factor both provide an estimate of pressure undershoot below the saturation pressure for flashing to commence.

The depressurization rate for nozzles was given by Abuaf *et al.* as

$$\Sigma' = \frac{G_c^3}{\rho^2}\frac{d(lnA)}{dz} + \Sigma'_0 \tag{7.4}$$

This expression for the depressurization rate is derived from the Bernoulli equation for steady frictionless flow. The additional transient component (Σ'_0) is equal to zero for steady flows. The depressurization rate at the nozzle throat was used by Abuaf *et al.* to determine the pressure differential to flashing inception.

Levy & Abdollahian (1982) used a slight modification to the Alamgir and Lienhard correlation based on the data of Reocreux (1974). Their final expression for the critical flow rate was virtually identical to those proposed by both Alamgir and Lienhard (1981) and Abuaf et al. (1983). In the Levy and Abdollahian model, the

flashing inception occurs when the liquid pressure reaches an amount below the saturation pressure corresponding to the liquid temperature. Levy and Abdollahian used an average decompression rate over the length of the nozzle.

$$\bar{\Sigma} = \frac{1}{4}(G_t + G_e)\left[\left(\frac{G}{\rho}\right)_t^2 - \left(\frac{G}{\rho}\right)_e^2\right] \Big/ \Delta z \tag{7.5}$$

The subscripts "t" and "e" correspond to throat and entrance, respectively, and Δz is the nozzle length. A critical assumption by Levy and Abdollahian (1982) is that a constant amount of superheat is maintained as the pressure decreases along the flow path through the nozzle, i.e., it did not account for any relaxation phenomena. They claimed the assumption of maintaining the liquid in non-equilibrium conditions is supported by the substantial relaxation times that could be inferred from the Marviken full-scale critical flow test data (Marviken, 1982).

The methods described for water by Alamgir and Lienhard (1981), Abuaf et al. (1983) and Levy and Abdollahian (1982) form the basis for the method described in this paper. The proposed method uses the Alamgir and Lienhard (1981) correlation (Equation (7.2)) to estimate the nozzle throat pressure. Contributions to the art include a description of how both nozzle geometry and fluid thermodynamics determine the bubble nucleation pressure at the nozzle throat. The nozzle converging section geometry determines the depressurization rate (Equation (7.4) with the transient component equal to zero). The method applies to both converging nozzles and sudden contractions by determining the point in the nozzle where the maximum depressurization rate occurs. In converging nozzles the change in flow area with respect to nozzle length determines the depressurization rate. In sudden contractions the depressurization rate is determined by fluid acceleration into the *vena contracta*. It is also recognized that the nucleation pressure estimated using Equation (7.2) represents the minimum nozzle throat pressure when rapid vaporization occurs at the nozzle throat. Sufficient pressure driving force must also be available for the depressurization due to acceleration to achieve the minimum nozzle throat pressure. If sufficient pressure driving force is not available, then the potential pressure-undershoot given by Equation (7.2) is not fully realized and an "approach to equilibrium" factor is utilized. The method is called herein the "bubble nucleation method".

8. Relaxation time

The conceptual model proposed for initially subcooled and saturated liquid flow through a nozzle is described by single-phase flow over the length of the nozzle with flashing, and choking, occurring at the nozzle throat. Application of the proposed model should be limited to situations where superheated fluid (i.e., metastable fluid) flow occurs over essentially the entire length of the nozzle and flashing occurs at the nozzle throat. Shin and Jones (1993) pointed out that treating the flashing inception as a single point has been previously justified since in many cases, such as converging–diverging nozzles, flashing occurs in a zone that is quite narrow. However, in other cases, such as constant-area flows with friction-dominated pressure profiles, the flashing may continue over a wider range of the nozzle length. This effect makes it important to determine range of applicability for the proposed method. In this regard, it is important to determine the relaxation time phenomena.

Moody (1975) and Fauske (1985) indicated for subcooled and saturated inlet conditions, flashing water-steam flow approaches equilibrium conditions for flow lengths larger than about 100 mm (4 in.). Kim (2015b) indicated the criterion could be 127 mm (5 in.) for subcooled and two-phase water, but should be changed to 305 mm (12 in.) for saturated water. Kim (2015b) also suggested an L/D ratio of 25 as a criterion for the transition from non-equilibrium choking to equilibrium choking for nozzle and pipe flashing water-steam flows. In contrast, Nilpueng and Wongwises (2009) studied the flow of HFC-134a through short tube orifices and observed metastable liquid flow at the tube central core surrounded by two-phase bubble flow followed by two-phase bubble flow after the metastable core disappeared. The length of the metastable core increased with the amount of subcooling but had disappeared before the end of the 15 mm (0.6 in.) long tubes used in their studies.

Sudi et al. (1994) studied the relaxation time of water in a 4.95 mm (0.19 in.) inside diameter by 1,055 mm (41.5 in.) long stainless steel tube. They defined the relaxation time as the time between the saturation inception point and the relaxation inception point. Effectively the saturation inception point is when the fluid reaches its bubble point pressure at the inlet temperature. The relaxation inception point was determined in their experiments by noting when the liquid temperature starts to decrease along with the liquid pressure. *Their data showed required relaxation lengths between 350 and 450 mm (14 and 18 in.) and corresponding relaxation times between about 55 and 85 ms.*

Downar-Zapolski et al. (1996) defined the relaxation time, Θ, in terms of quality for use in the Homogeneous Relaxation Model (HRM).

$$\frac{Dx}{Dt} = \frac{\partial x}{\partial t} + u\frac{\partial x}{\partial z} = -\frac{x - x_E}{\theta} \tag{8.1}$$

Locally, in a Lagrangian description of the flow, the relaxation equation exhibits an exponential approach to equilibrium from an initial state x_0.

$$x = x_E - (x_E - x_0)exp\left(\frac{-t}{\theta}\right) \tag{8.2}$$

Downer-Zapolski *et al.* indicated that for θ = 1 s, the predictions of the HRM are equivalent to the Homogeneous Frozen Model (HFM) and for θ = 0.001 s (1 ms), the HRM predictions are equivalent to the Homogeneous Equilibrium Model (HEM). *An implication for subcooled and saturated liquid flow in nozzles is that relaxation time, not length or length/diameter ratio, should be the criterion for approach to equilibrium.*

9. Thermodynamic considerations

The amount of superheating upon rapid depressurization of a subcooled or saturated liquid is constrained by the fluid thermodynamic properties. A depressurization diagram is illustrated in Fig. 9.1 for water. The upper (or leftmost) curve represents the water saturation pressure and the lower (or rightmost) curve represents the liquid thermodynamic stability limit, called the spinodal curve. The curves in between represent the expected pressure-undershoot below the saturation pressure using the Alamgir and Lienhard correlation (Equation (7.2)). A thermodynamic path for near isothermal rapid depressurization, such as experienced during isentropic expansion of a subcooled liquid, is illustrated starting at point A and ending at point B. For small depressurization rates, the amount of pressure-undershoot before nucleation occurs is small and flashing occurs near the saturation pressure. As the depressurization rate increases, the amount of pressure-undershoot also increases and flashing occurs at pressures further below the saturation pressure. At an extremely high depressurization rate, the amount of pressure-undershoot is limited by the spinodal pressure. Note that as the nozzle inlet temperature (point A) approaches the thermodynamic critical temperature, the spinodal curve approaches the vapor pressure curve and thus decreases the maximum possible amount of

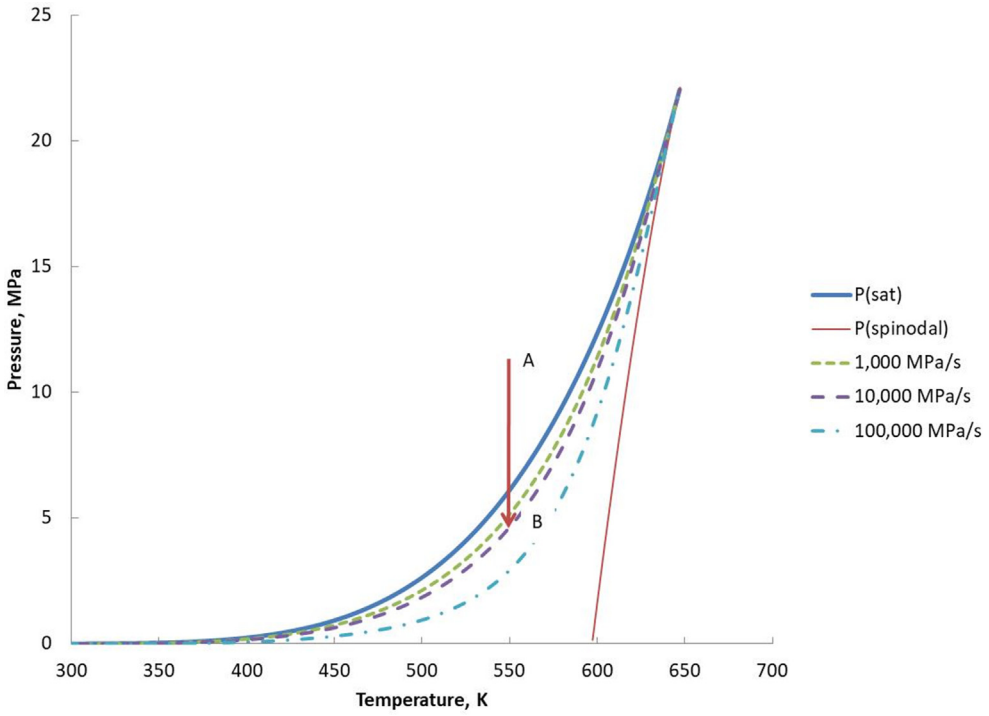

Fig. 9.1. Water Depressurization Diagram.

pressure-undershoot. These observations are important for non-equilibrium liquid flow because, for a fixed inlet pressure, as the amount of pressure undershoot below the vapor pressure increases the pressure differential to drive the flow increases and thus the flow rate also increases.

Given an undershoot pressure equal to the nozzle throat pressure, Equation (9.1) is used to calculate a Burnell C factor for use in Equations 4.5 or 4.6.

$$C = 1 - \frac{P_u}{P_s} \tag{9.1}$$

Fig. 9.2 illustrates the Burnell C factor diagram for saturated water developed from the Alamgir and Lienhard correlation (Equation (7.2)) and Equation (9.1). Comparison of Fig. 9.2 with the Weisman and Tentner (1978) correlation (Fig. 4.3) shows the Weisman and Tenter correlation fits between the curves for 1,000 and 10,000 MPa/s (0.01 and 0.1 Matm/s).

It is very important to distinguish between the undershoot pressure as estimated from the Alamgir and Lienhard correlation and the flashing pressure at the nozzle throat as is discussed later in the analysis of the Sozzi and Sutherland (1975) *data.* The pressure-undershoot value estimated using the Alamgir and Lienhard correlation represents the maximum possible departure from equilibrium. The minimum possible departure from equilibrium is of course zero, i.e., flashing at the fluid saturation pressure. The pressure at which flashing occurs at the nozzle throat is between these two extremes and is determined by the fluid initial conditions and the nozzle geometry.

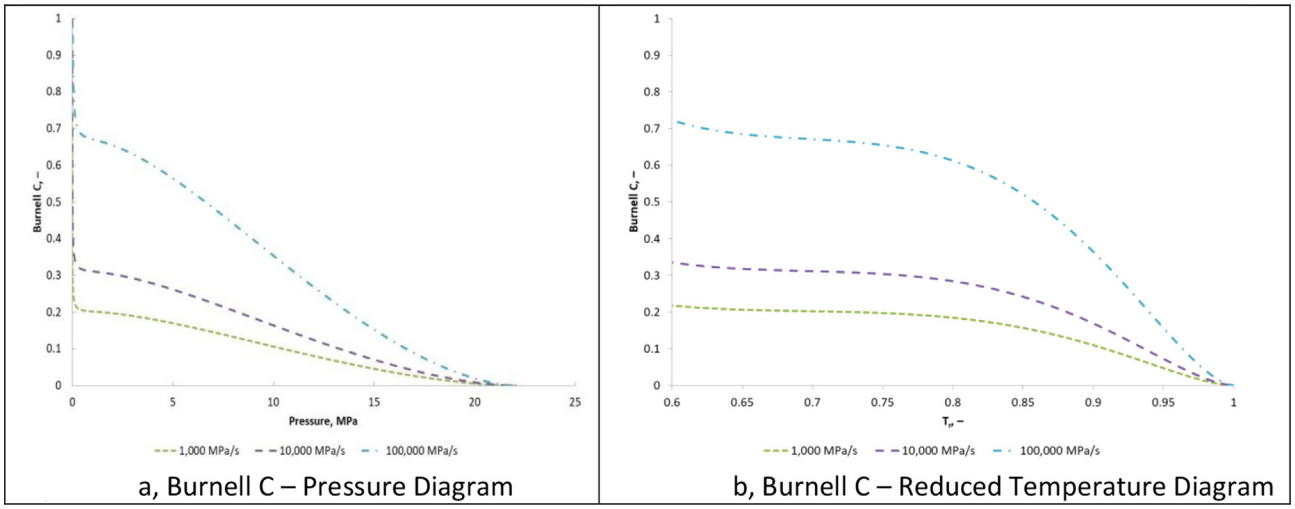

Fig. 9.2. Water Burnell C Factor Diagrams.

10. Sozzi and Sutherland water flow data analysis

Sozzi and Sutherland conducted a series of blowdown experiments to measure the critical flow rate of water through various nozzles. The experiments included subcooled, saturated and two-phase flow entering the nozzles. The data analysis herein is only applicable to subcooled or saturated liquid nozzle inlet flows.

The Sozzi and Sutherland experiments were performed by discharging high pressure water from a vessel to atmosphere through various nozzles. The nozzles were mounted with the entrance to the nozzle flush with the inside wall of the blowdown vessel to minimize irreversible pressure losses of the fluid as it accelerated from the stagnation condition to the minimum cross-sectional area of the nozzles. Sozzi and Sutherland's "nozzle 2" was chosen for this analysis (Fig. 10.1) because its geometry is representative of pressure relief device nozzles. Note in the Sozzi and Sutherland terminology, the "length" of the nozzle refers to the length of the straight section downstream of the converging section. For example, a "zero" length nozzle does not actually have zero length; the actual length is the converging section length.

The throat pressures were not provided in the Sozzi and Sutherland data so throat pressures calculated using the Burnell equation (Equation (4.6)) were compared to the bubble nucleation pressures calculated using the Alamgir and Lienhard correlation (Equation (7.2)). The shape of the converging section is required in order to calculate the depressurization rate, but it was not specified in the Sozzi and Sutherland article. It was, however, described as a "rounded inlet," as depicted in Fig. 10.1. For convenience, it was assumed the shape of the nozzle inlet could be represented by a sine function. The depressurization rate associated with steady-state acceleration of an incompressible fluid was then calculated as follows. The nomenclature is illustrated in Fig. 10.2.

$$h = h_0 sin\left(\frac{\pi z}{2L}\right) \tag{10.1}$$

$$d_c = D - 2h_0 sin\left(\frac{\pi z}{2L}\right) \tag{10.2}$$

$$A = \frac{\pi}{4}\left[D - 2h_0 sin\left(\frac{\pi z}{2L}\right)\right]^2 \tag{10.3}$$

$$u = \frac{\dot{m}}{\rho A} = \frac{dz}{dt} \tag{10.4}$$

The Sozzi and Sutherland nozzle 2 dimensions are D = 43.2 mm, d = 12.7 mm, h_0 = 15.25 mm and L = 44.5 mm. Upon rearranging and integrating the velocity equation, Equation (10.4), from time = 0 to t and z = 0 to L, the residence time in the converging section is found to be

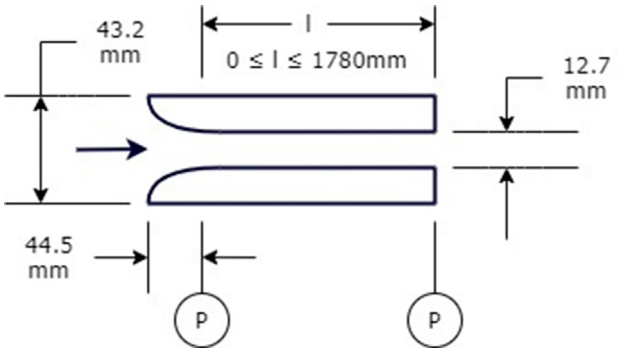

Fig. 10.1. Sozzi and Sutherland (1975) Nozzle 2 with Length of Straight Tube.

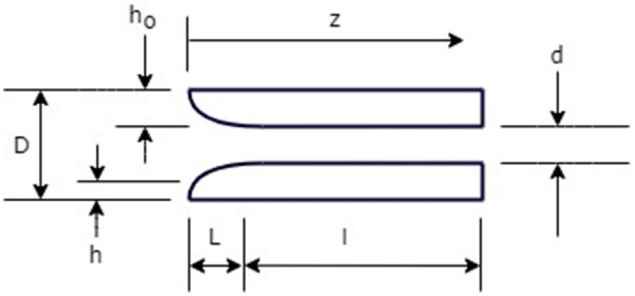

Fig. 10.2. Nomenclature Applied to Sozzi and Sutherland (1975) Nozzle 2.

$$\tau = \frac{\rho}{\dot{m}}\frac{\pi}{4}\int_0^L \left[D - 2h_0 sin\left(\frac{\pi z}{2L}\right)\right]^2 dz \tag{10.5}$$

$$\tau = \frac{\rho L}{\dot{m}}\left(\frac{\pi}{4}D^2 + \frac{\pi}{2}h_0^2 - 2Dh_0\right) \tag{10.6}$$

The acceleration pressure drop of the yet non-flashing incompressible liquid flow in the converging section is calculated using the steady-state differential mechanical energy balance (Equation (4.1))

$$-\frac{dP}{dz} = \rho u \frac{du}{dz} \tag{10.7}$$

Upon combination with the incompressible continuity equation ($\frac{du}{u} = -\frac{dA}{A}$) and multiplication by the velocity, Equation (10.7) becomes

$$\frac{dP}{dt} = u\frac{dP}{dz} = \frac{\rho u^3}{A}\frac{dA}{dz} = \frac{\dot{m}^3}{\rho^2 A^4}\frac{dA}{dz} \tag{10.8}$$

Equation (10.8) is equivalent to Equation (7.4) with the transient component equal to zero. From Equation (10.3), the derivative of the area is

$$\frac{dA}{dz} = -\frac{\pi^2 h_0}{2L}\left[D - 2h_0 sin\left(\frac{\pi z}{2L}\right)\right] cos\left(\frac{\pi z}{2L}\right) \tag{10.9}$$

The final relationship between the depressurization rate and nozzle geometry is obtained by combining Equations (10.8) and (10.9).

$$\frac{dP}{dt} = -\frac{\dot{m}^3}{\rho^2 A^4}\frac{\pi^2 h_0}{2L}\left[D - 2h_0 sin\left(\frac{\pi z}{2L}\right)\right] cos\left(\frac{\pi z}{2L}\right) \tag{10.10}$$

The depressurization rate to use in the Alamgir and Lienhard correlation, Equation (7.2), is found by determining the maximum depressurization rate given by Equation (10.10). The maximum depressurization rate determines the lower bound on the throat pressure. The location of the maximum depressurization rate is obtained by differentiating Equation (10.10) with respect to z and setting that result equal to zero to obtain Equation (10.11). The location of the maximum depressurization rate is obtained by solving Equation (10.11) for z.

$$D - 2h_0 sin\left(\frac{\pi z}{2L}\right) = 14h_0 cos\left(\frac{\pi z}{2L}\right) cot\left(\frac{\pi z}{2L}\right) \tag{10.11}$$

For the Sozzi and Sutherland nozzle 2 geometry, the location of the maximum depressurization rate is found to occur at z = 37.656 mm (1.471 in.). The depressurization rate at that location is found using Equations (10.10) and (10.12) and then used in the Alamgir and Lienhard correlation to estimate the pressure-undershoot.

$$\Sigma' = \left(-\frac{dP}{dt}\right)_{max} \tag{10.12}$$

An example depressurization rate calculation result is illustrated in Fig. 10.3. The distance on the abscissa is from the nozzle entrance to the end of the converging section. One can see in the illustration the peak depressurization rate occurs over a short distance in the nozzle converging section.

The throat pressures calculated using the Burnell equation for the various nozzle lengths were overlaid on the water depressurization diagram (Fig. 10.4). One can see the general trend is as expected. More detailed comparisons for l = 0 mm (0 in.) and l = 12.7 mm (0.5 in.) are illustrated in Figs. 10.5 and 10.6. The agreement between the bubble nucleation method and the Burnell method indicates acceleration losses are a major contributor to the amount of fluid superheat, i.e., metastability. However, for longer nozzle lengths a more detailed investigation reveals another phenomenon that must be considered.

Figure 10.7 depicts the combined effects of initial subcooling and depressurization rates on the resulting deviation from equilibrium at the nozzle exit. The results are illustrated for the 114.3 mm (4.5 in.) long nozzle. The 114.3 mm nozzle length data was selected to demonstrate that non-equilibrium conditions can still occur at the exit of nozzles greater than 100 mm in length. For small depressurization rates or for large degrees of initial subcooling, the bubble nucleation pressures, and thus the nozzle throat pressures, approach the fluid saturation pressures; namely, the Burnell C factors approach zero. For large depressurization rates or for small degrees of initial subcooling, the bubble nucleation pressures, and thus the nozzle throat pressures, approach the bubble nucleation pressures predicted by the Alamgir and Lienhard correlation.

In Fig. 10.7a, the depressurization rate is small (ca. 2,500 MPa/s), compared to that in Fig. 10.7b and c (ca. 3,500 MPa/s) as indicated by the peak depressurization rate located at z = 37.656 mm. The amount of initial subcooling is also small as indicated by the small difference between the saturation pressure and the pressure at the nozzle inlet (z = 0). The local fluid pressure decreases due to acceleration as it flows through the nozzle converging section, as indicated by the solid line. The nozzle throat pressure approaches the Alamgir and Lienhard nucleation pressure, P_n, because the local pressure is smaller than the vapor pressure when the fluid has reached its maximum depressurization rate. Thus, in the case of shorter nozzles with larger peak depressurization rates, the nozzle throat pressures approach the Alamgir and Lienhard nucleation pressure.

Fig. 10.7c represents the opposite extreme of a large amount of subcooling with a large peak depressurization rate. For this case, because of the large degree of initial subcooling, the local pressure is still larger than the fluid vapor pressure at the location of maximum depressurization rate. Consequently, in this case, the nucleation pressure at the nozzle throat approaches the fluid vapor pressure.

Fig. 10.7b illustrates an intermediate case where the depressurization rate is large and the local pressure at the location of maximum depressurization rate is near the fluid vapor pressure. In this case the flashing pressure at the nozzle throat is between the two extremes. *As illustrated, the Alamgir and Lienhard nucleation pressure can be considered the maximum potential amount of non-equilibrium given enough pressure driving force to cause it to occur.*

The non-equilibrium phenomena shown in Fig. 10.7 can be quantified by defining an "efficiency" to adjust the pressure-undershoot determined by the Alamgir and Lienhard correlation. The "driving force" for non-equilibrium is the difference between the fluid saturation pressure and the local pressure at the location

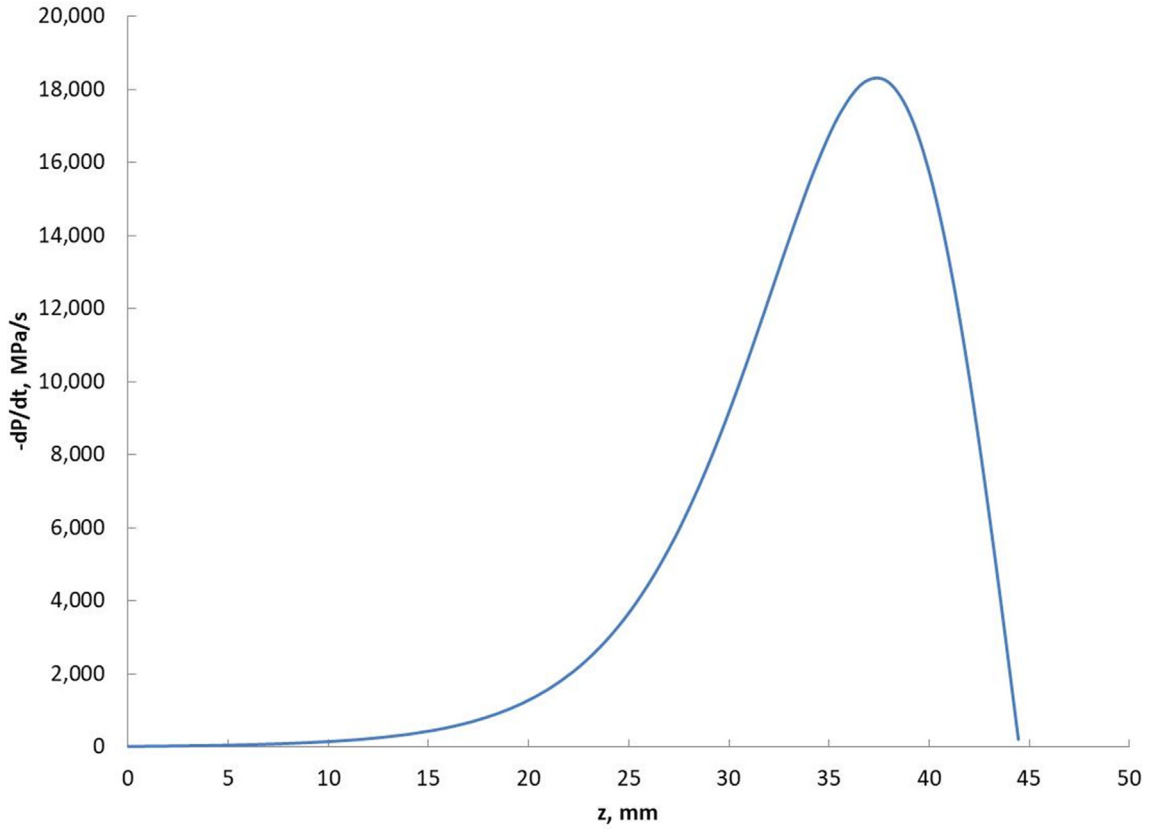

Fig. 10.3. Example Calculated Water Depressurization Rate for Sozzi and Sutherland (1975) Nozzle 2 for l = 0 mm (0 in.)

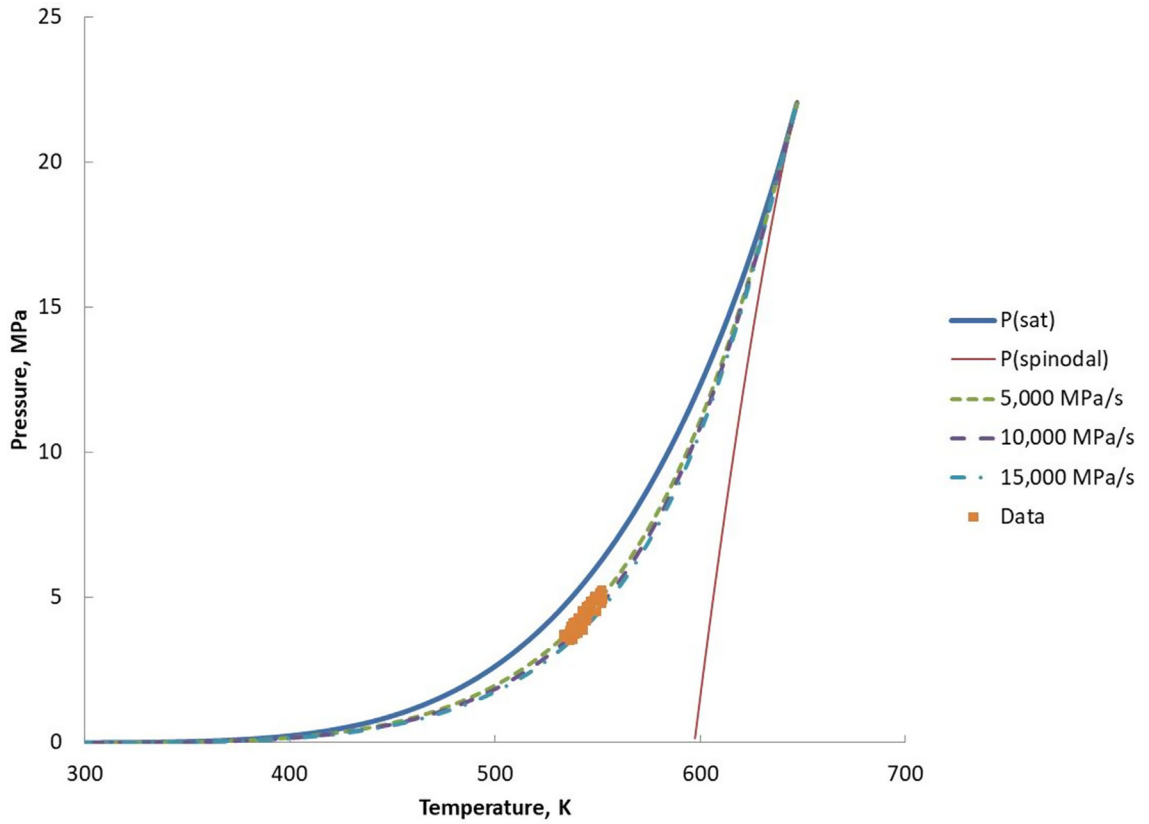

Fig. 10.4. Sozzi and Sutherland (1975) Water Depressurization Diagram.

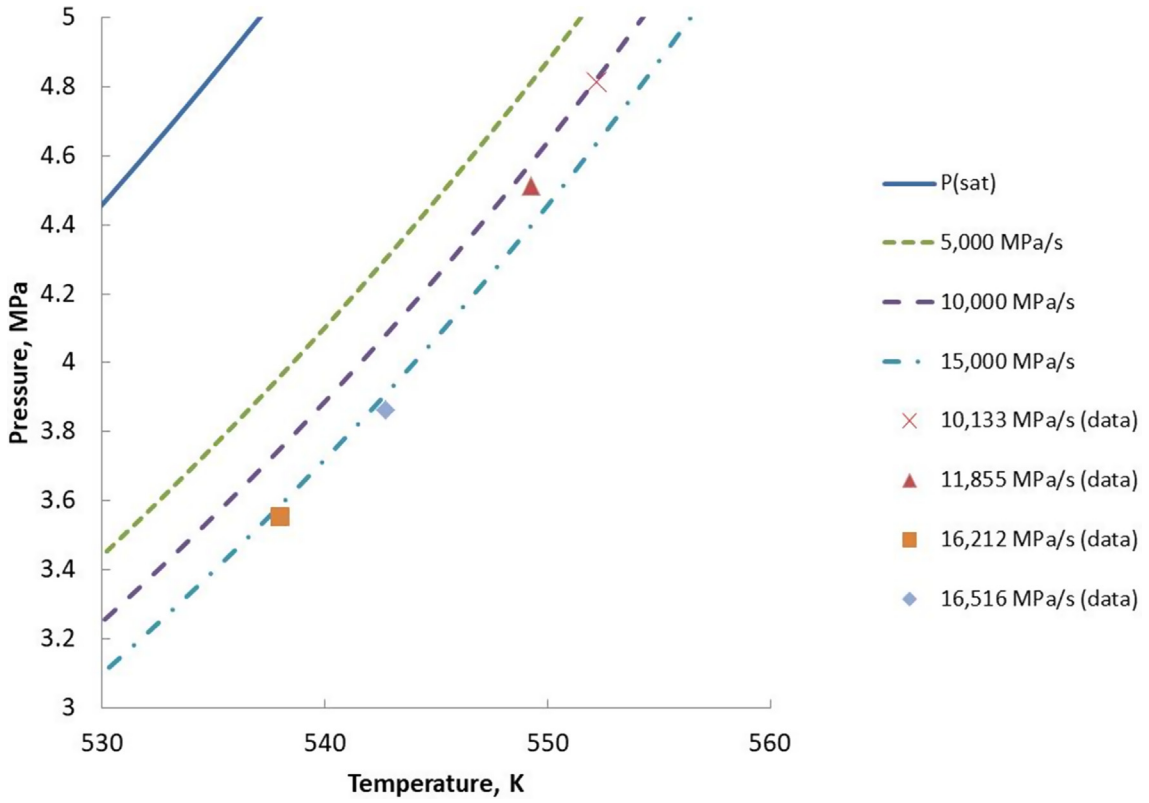

Fig. 10.5. Sozzi and Sutherland (1975) Depressurization Diagram for l = 0 mm (0 in.)

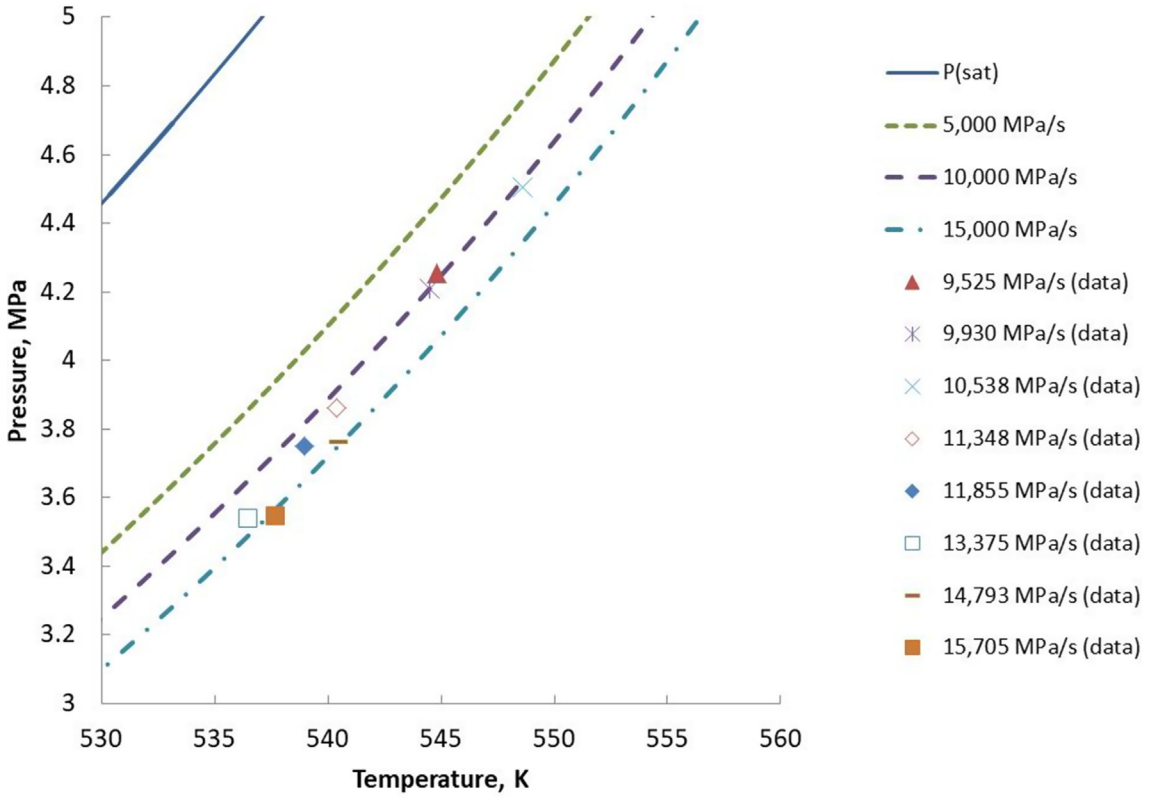

Fig. 10.6. Sozzi and Sutherland (1975) Depressurization Diagram for l = 12.7 mm (0.5 in.)

of the maximum depressurization rate. The "efficiency" can be thought of as an approach to equilibrium.

$$(P_{sat} - P_{n,relaxed}) = \eta(P_{sat} - P_{n,A-L}) \tag{10.13}$$

The nucleation pressure calculated using the Alamgir and Lienhard correlation is adjusted with the approach to equilibrium "efficiency" to determine the nozzle throat pressure, $P_{n,relaxed}$. The nozzle throat pressure is then used in Equation (10.14) to estimate the mass flux.

$$G = \sqrt{\frac{2\rho_0(P_0 - P_{n,relaxed})}{1 + f_D \frac{l}{d}}} \tag{10.14}$$

In practice a trial-and-error solution is required because the maximum depressurization rate and the local pressure at the location of the maximum depressurization rate are not known *a priori*.

The approach to equilibrium efficiency is depicted as a function of the "driving force" for nucleation in Fig. 10.8. A solid line is drawn at an efficiency of one to indicate values larger than one are not used. The reasons for values greater than one obtained during the data analysis are described in the next paragraph.

The premise for the use of the Bernoulli or Burnell equations to estimate nozzle critical flow is that rapid vaporization occurs predominately near the nozzle exit. The difference between the two equations is that boiling is "delayed" below the saturation pressure when using the Burnell equation. A nucleation delay time of 1 ms has been reported (see for example Sozzi and Sutherland (1975) "Discussion of Results"). With a 1 ms nucleation delay time, flashing almost certainly occurs downstream of the Sozzi and Sutherland "zero" length nozzle and likely also occurs downstream of the 12.7 mm (0.5 in.) long nozzle. The residence time in the straight section of the 12.7 mm (0.5 in.) long nozzle is 0.14 – 0.17 ms assuming all liquid flow. The transition between flashing downstream of the nozzle and flashing in the nozzle likely occurs in the 38.1 mm (1.5 in.) long nozzle, with flashing possibly occurring downstream of the nozzle for the most subcooled data points and within the nozzle for the least subcooled data points. The data points in Fig. 10.8 having efficiencies greater than one are for the shortest nozzles where flashing is likely occurring downstream of the nozzles and are thus not applicable for the current model premise.

The nozzle throat pressures were not generally provided in the Sozzi and Sutherland (1975) data so the nozzle throat pressure calculated using Equation (10.13) (notated as $P_{nucleation}$ to represent use of the nucleation theory) is compared to the nozzle throat pressure using the Burnell equation in Fig. 10.9. The agreement is generally acceptable. To be clear, experimental values of the stagnation pressure and mass flux were used in Equation (4.6) to calculate the Burnell C factor and the "Burnell" throat pressure along with the equation $P_t = (1 - C)P_s$. Disagreement between the two calculation methods occurs for the two shortest nozzles (0 and 12.7 mm) when flashing takes place downstream of the nozzle.

Two comparisons of the mass fluxes calculated using the bubble nucleation method and the experimental data are found in Fig. 10.10. Again the bubble nucleation method provides generally good agreement with the measured data except for the shortest nozzles. Calculation of the Burnell C factor is straightforward given the nozzle throat pressure. The Burnell C factor calculated using the nucleation theory is compared to that calculated using the Burnell equation in Fig. 10.11. Again, when choking is concurrent with flashing at the nozzle throat, the two methods agree. The exceptions are when choking occurs downstream of the nozzle throat in the two shortest nozzles.

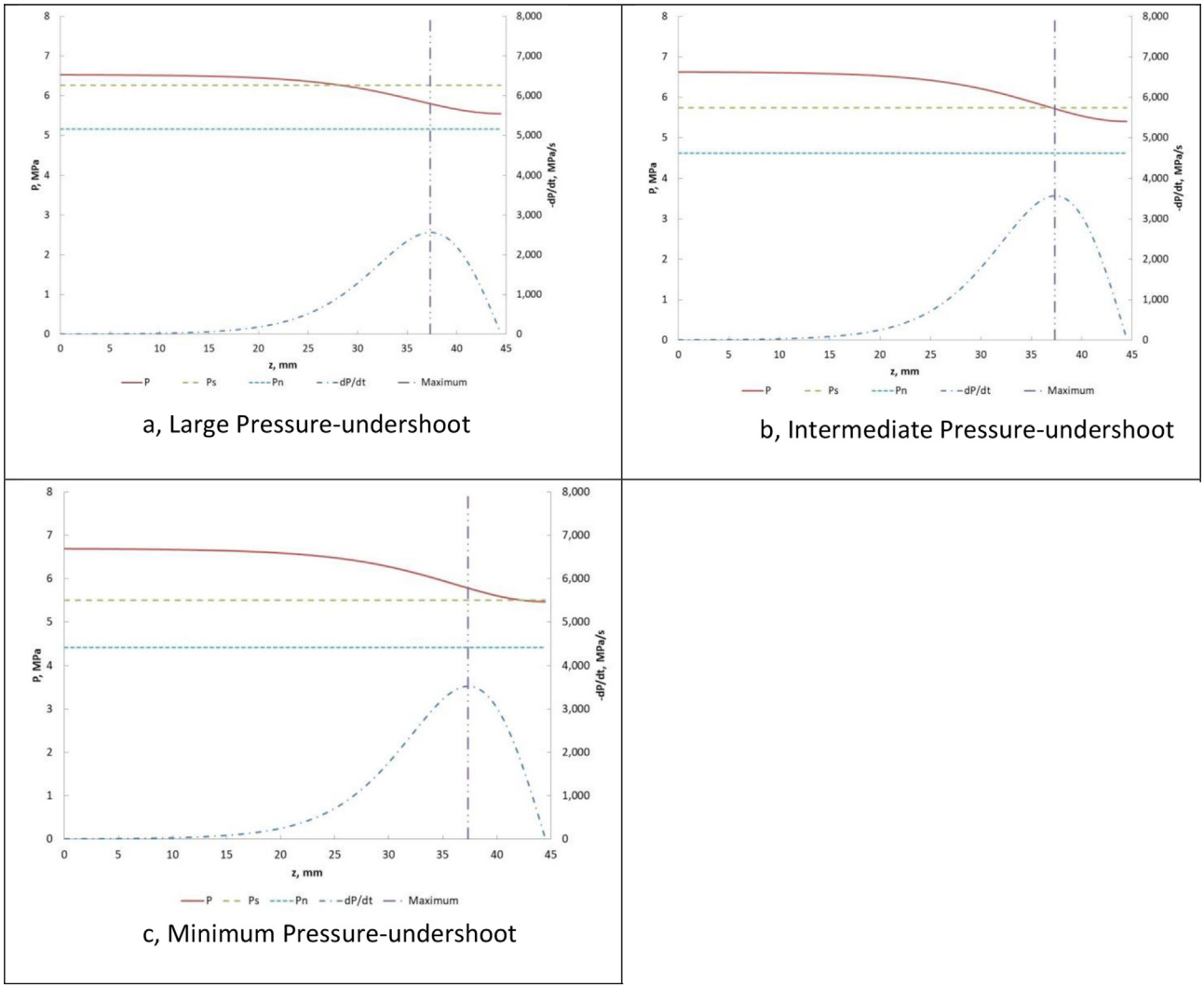

Fig. 10.7. Pressure-undershoot at Point of Maximum Acceleration for l = 114.3 mm (4.5 in.)

11. Conclusions

Unification of bubble nucleation kinetics and thermodynamic stability analyses used to describe Rapid Phase Transitions (RPT), Boiling Liquid Expanding Vapor Explosions (BLEVE) and flow through nozzles provides a method to quantify non-equilibrium effects on calculated nozzle choking pressures and critical mass flow rates. It was shown that the deviation from equilibrium in converging nozzles is determined by the maximum depressurization rate due to fluid acceleration combined with the amount of initial subcooling of the entering fluid. The proposed method addresses known deficiencies of the Homogeneous Equilibrium Model for flow of saturated or slightly subcooled liquid through nozzles. Conclusions from thermodynamic considerations and the study of the Sozzi and Sutherland (1975) data are:

1. Nozzle flow can approach equilibrium flow when:
2. initial fluid temperature approaches the critical temperature because the amount of superheating due to rapid depressurization is constrained by the spinodal curve, e.g., less superheating is possible due to thermodynamic instability
3. small rates of depressurization due to fluid acceleration occur, e.g., small available pressure driving force or appropriately rounded nozzle inlet geometries limit the maximum depressurization rate
4. the local pressure is above the fluid saturation pressure at the location in the nozzle where the maximum depressurization rate occurs, e.g., at a given temperature, as the amount of subcooling increases due to increasing pressure, greater acceleration losses are required to decrease the local pressure to below the vapor pressure at the location of the maximum depressurization rate
5. long residence time in the nozzle straight section downstream of the converging section allows enough time for fluid relaxation
6. Otherwise, non-equilibrium flow should be considered for saturated or slightly subcooled liquid flow into a nozzle.
7. The inlet geometry of short nozzles plays a key role in the amount of superheating because the inlet geometry determines the maximum rate of depressurization for a given pressure driving force. Empirical correlations developed from data using nozzles with rounded inlets may not be applicable to nozzles with sharp-edged inlets because of geometry effects. In the case of rounded inlets (wherein no *vena contracta* is formed), the change in area with respect to distance (dA/dz) determines the maximum rate of depressurization. In the case of square-edged inlets, the fluid acceleration from the point of fluid detachment at the contraction plane to the *vena contracta* determines the maximum rate of depressurization. Where a *vena contracta* is formed, it is important to note whether fluid

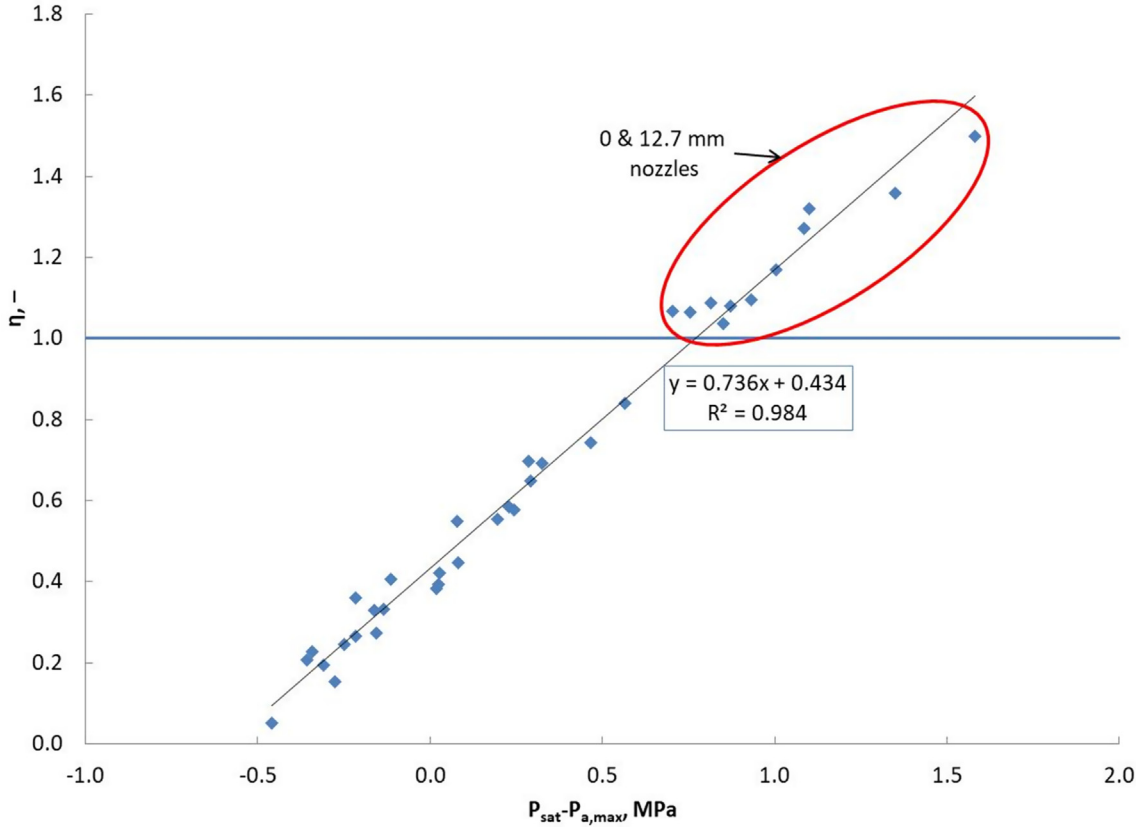

Fig. 10.8. Efficiency of Converting Potential Bubble Nucleation Pressure to Nozzle Throat Pressure.

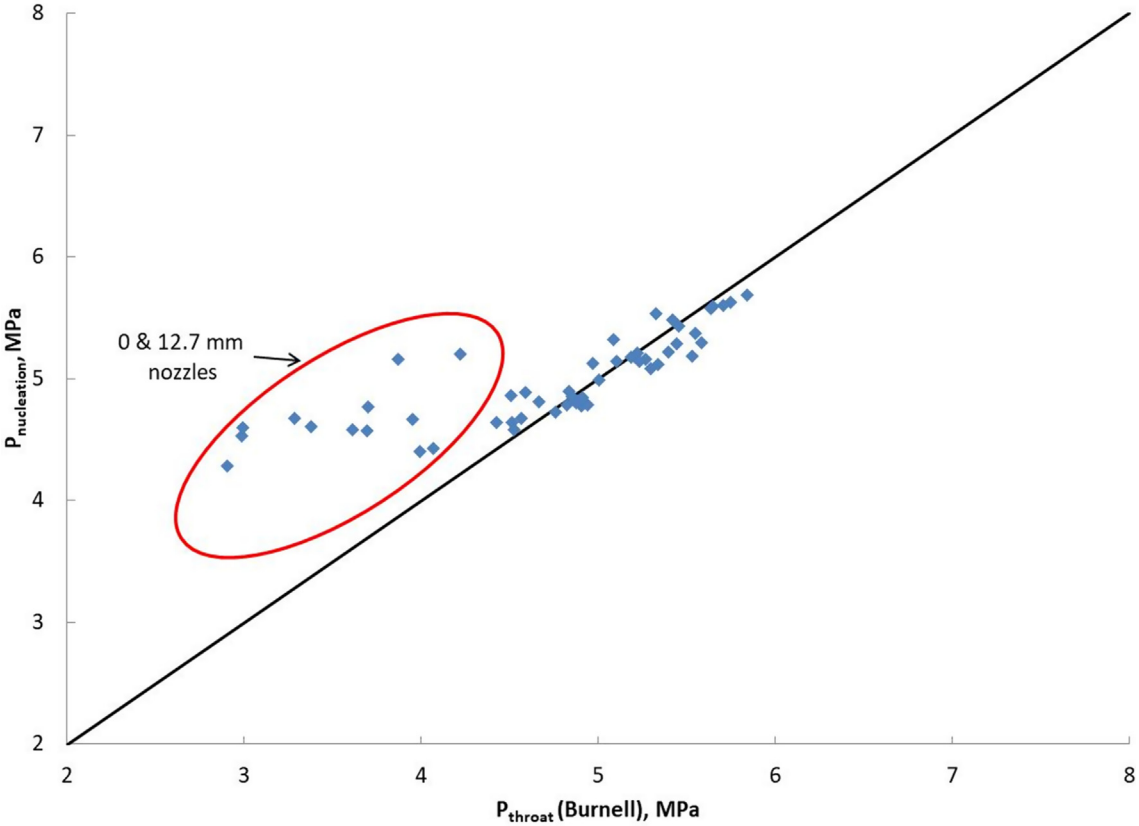

Fig. 10.9. Sozzi and Sutherland (1975) Nozzle 2 Outlet Pressures.

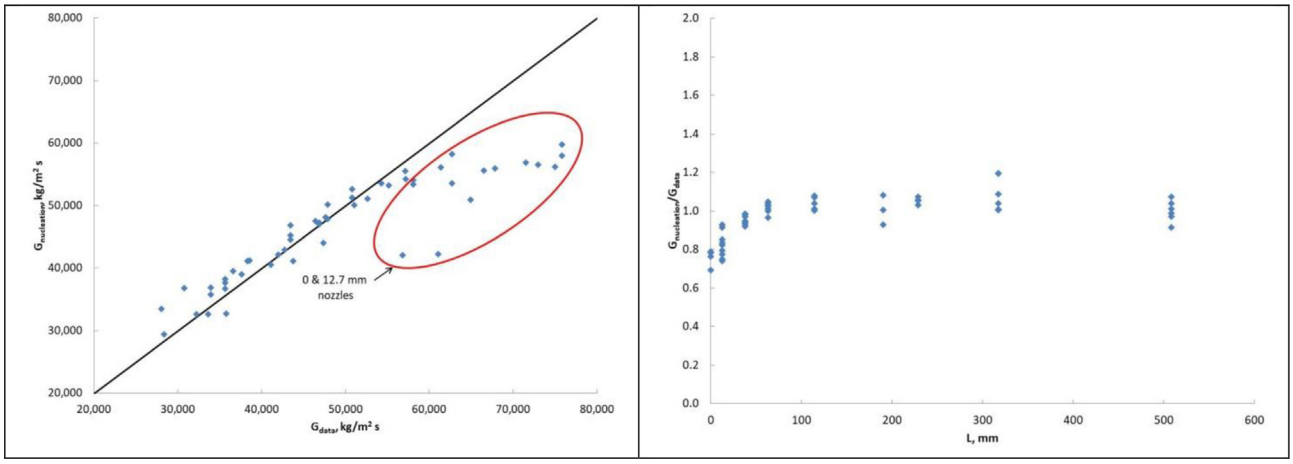

Fig. 10.10. Sozzi and Sutherland (1975) Nozzle 2 Mass Fluxes.

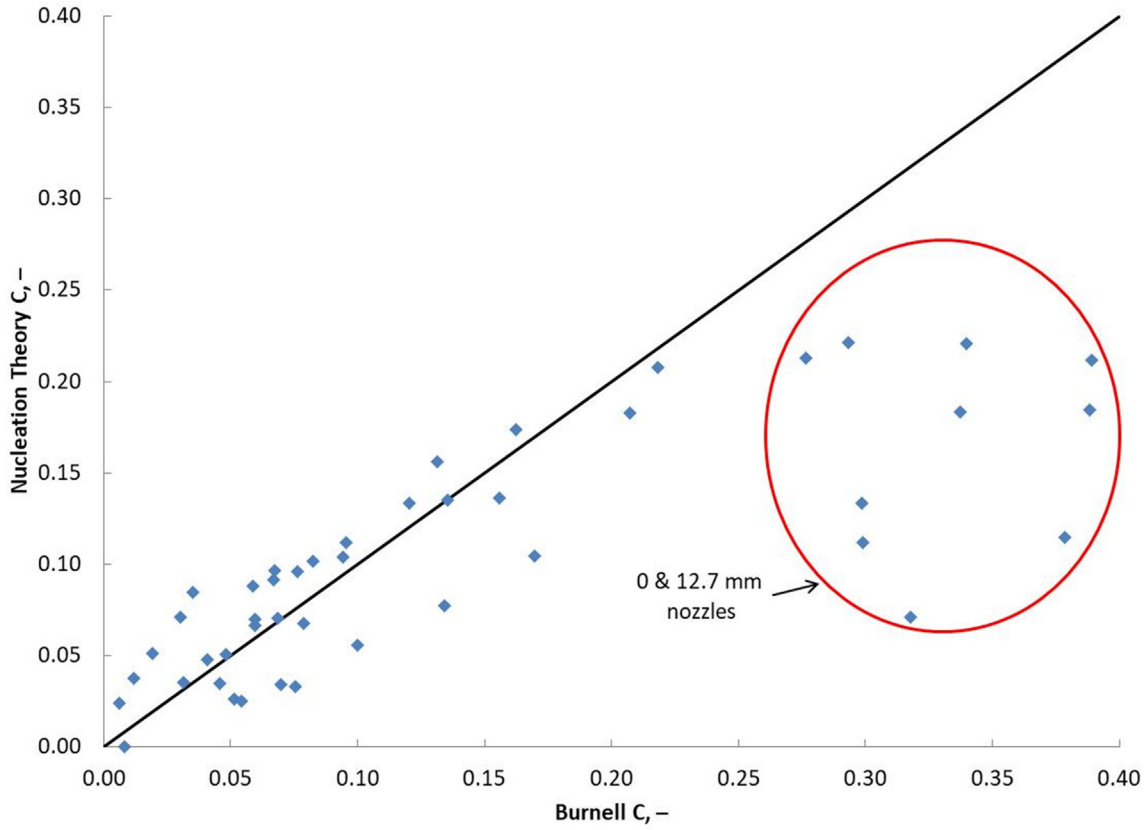

Fig. 10.11. Sozzi and Sutherland (1975) Nozzle 2 Burnell C Factor.

reattachment downstream of the *vena contracta* occurs. In the case of short nozzles where fluid reattachment does not occur, the relevant flow area is the *vena contracta* cross-sectional area. Also without flow reattachment, there are no frictional losses along the nozzle wall.

12. Summary

A bubble nucleation method to estimate the flow rate of saturated and slightly subcooled liquids through "short" nozzles is proposed. The premises of the method are:

1. The available pressure driving force causes rapid depressurization of the fluid at the nozzle inlet due to the reduction in area available for flow determined by the nozzle geometry. The method is applied to both converging and square-edged inlet geometries by following the flow streamlines.
2. The *potential* pressure-undershoot is determined using a pressure-undershoot correlation at the point in the nozzle where the maximum rate of depressurization occurs.
3. The *realized* pressure-undershoot is determined by adjusting the *potential* pressure-undershoot with an approach to equilibrium "efficiency" based on the amount of superheating at the

location in the nozzle where the maximum depressurization rate occurs. The nozzle throat pressure is determined by the realized pressure-undershoot value.
4. Rapid vaporization occurs essentially at the nozzle throat after a bubble nucleation time delay resulting in choking essentially at the nozzle throat.

The applicable ranges of the proposed method are summarized as follows:

1. The single phase Bernoulli and Darcy–Weisbach equations are used to describe the pressure drop of the metastable fluid through the nozzle, thus the metastable fluid should be considered incompressible.
2. Upon depressurization, the Alamgir and Lienhard correlation is used to determine the pressure-undershoot. The Alamgir and Lienhard correlation was developed for

$$0.62 \le T_r \le 0.935 and 0.004 \le \Sigma' \le 1.8 Matm/s (405 \le \Sigma' \le 182,000 MPa/s)$$

3. Nucleation should commence within the nozzle. Yoon *et.al* (2006) suggested a nucleation delay time of about 1 ms. The residence time in the straight section of the 12.7 mm (0.5 in.) long Sozzi and Sutherland Nozzle 2 was less than 0.2 ms indicating nucleation initiated downstream of the nozzle. The residence time in the straight section of the 38.1 mm (1.5 in.) long Sozzi and Sutherland nozzles was 0.5 – 0.7 ms, and that data fit the correlation, indicating perhaps 1 ms is a conservative estimate for the minimum nozzle residence time.
4. Rapid vaporization, and coincident choking, is premised to occur essentially at the nozzle throat, thus the method is limited to modeling "short" nozzles. The definition of "short" will certainly depend on the amount of initial fluid subcooling, the maximum depressurization rate, the fluid relaxation time and the nozzle geometry. Sozzi and Sutherland (1975) suggested nozzle flow approaches equilibrium flow, as calculated using the Homogeneous Equilibrium Method (HEM), for nozzles around 127 mm (5 in.) long. The residence time for the 114.3 mm (4.5 in.) long Nozzle 2 data set was about 2 ms. The proposed bubble nucleation method fit the Sozzi and Sutherland Nozzle 2 data for Nozzles as long as 228.6 mm (9 in.), corresponding to about 5 ms residence time. For longer nozzles the exiting fluid was predicted to be saturated, indicating the model may be valid for nozzle residence times as long as 5 ms.

The proposed method was developed with data from experiments using water, but bubble nucleation theory indicates applicability to other pure components with proper scaling of the Gibbs number. Development and validation of Gibbs number scaling methodology is an area of proposed future research. Wide boiling mixtures are unlikely to experience rapid vaporization, indicating application of the method is likely limited to pure components and perhaps mixtures with a narrow boiling range. Finally, the method was developed using data from experiments in which acceleration pressure losses dominated and rapid vaporization occurred essentially at the nozzle throat. In nozzles with friction dominated pressure profiles, flashing may occur over a wide range of the nozzle length and other methods such as the HNE and DEM should be considered.

13. Recommendations for further work

Recommendations for further work are:

1. The Alamgir and Lienhard (1981) pressure-undershoot correlation was developed from rapid depressurization experimental data, for example see Alamgir, et al. (1980). The rapid depressurization experiments typically involved filling a closed tube with water, heating and pressurizing to the desired initial conditions, "bursting" open the outlet end of the tube and then measuring the depressurization rate and pressure-undershoot. Similar experiments with imposed backpressures are recommended to quantify the back pressure effect on depressurization rate and amount of pressure-undershoot. These experiments are recommended with a variety of other chemicals (including mixtures) to verify the Gibbs number composition dependency.
2. Critical flow experiments with nozzles having various inlet geometries, e.g., varying the radius of curvature and beta ratio, are recommended to validate the interpretation of geometric effects changing the fluid streamlines and use of the maximum depressurization rate in the pressure-undershoot correlation. These experiments should also include a variety of other chemicals (including mixtures) to validate application to nozzle flow calculations of the pressure-undershoot correlation and the approach to equilibrium correlation. The nozzle lengths should also be varied to determine the location of flashing inception and the role of the boiling nucleation time delay.

CRediT authorship contribution statement

Gregory G. Hendrickson: Conceptualization, Methodology, Formal analysis, Investigation, Writing – original draft, Visualization. **Daniel K. Smith:** Conceptualization, Formal analysis, Writing – review & editing. **Robert N. D'Alessandro:** Conceptualization, Data curation, Writing – review & editing. **Georges A. Melhem:** Conceptualization, Methodology, Resources, Software, Validation, Formal analysis, Investigation. **Marc E. Levin:** Conceptualization, Data curation, Validation, Visualization. **Harold G. Fisher:** Writing – review & editing. **Leonid Korelstein:** Writing – review & editing.

Declaration of Competing Interest

The authors declare that they have no known competing financial interests or personal relationships that could have appeared to influence the work reported in this paper.

References

Abuaf, N., Jones Jr., O.C., Wu, B.J.C., 1983. Critical Flashing Flows in Nozzles with Subcooled Inlet Conditions. ASME J. Heat Transfer 105, 379–383. https://doi.org/10.1115/1.3245589.
Alamgir, M.d., Kan, C.Y., Lienhard, J.H., 1980. An Experimental Study of the Rapid Depressurization of Hot Water. ASME J. Heat Transfer 102, 433–438. https://doi.org/10.1115/1.3244318.
Alamgir, M.d., Lienhard, J.H., 1981. Correlation of Pressure Undershoot During Hot-Water Depressurization. ASME J. Heat Transfer 103, 52–55. https://doi.org/10.1115/1.3244429.
Angelo, E., Angelo, G., Andrade, D.A., 2012. A Mathematical Model for Metastable Condition Determination in Highly Flashing Liquid Flows Through Expansion Devices. Nucl. Eng. Design 242, 257–266. https://doi.org/10.1016/j.nucengdes.2011.09.039.
Bartosiewicz, Y., Seynhaeve, J.M., and Serre, G., "Delayed Equilibrium Model and Validation Experiments for Tw-Phase Choked Flows Relevant to LOCA", NURETH14, Toronto, Canada, September 25-30, 2011.
Benedict, R.P., 1980. Fundamentals of Pipe Flow. John Wiley and Sons, New York.
Benjamin, M.W., Miller, J.G., 1942. "The Flow of a Flashing Mixture of Water and Steam through Pipes. Trans ASME 64, 657–664.
Brennen, C.E., "Cavitation and Bubble Dynamics", Oxford University Press, New York (1995), https://authors.library.caltech.edu/25017/5/BUBBOOK.pdf.
Burnell, J.G., "Flow of Boiling Water through Nozzles, Orifices, and Pipes", Engineering, 164 (1947), 527–576.
De Lorenzo, M., 2018. Modeling and Numerical Simulation of Metastable Two-Phase Flows. Doctoral Thesis from the University of Paris-Saclay prepared at the Ecole Polytechnique.
Diener, R., Schmidt, J., 2004. Sizing of Throttling Device for Gas/Liquid Two-Phase Flow Part 1: Safety Valves. Process Saf. Prog. 23 (4), 335–344. https://doi.org/10.1002/prs.10034.

Diener, R., Schmidt, J., 2005. Sizing of Throttling Device for Gas/Liquid Two-Phase Flow Part 2: Control Valves, Orifices and Nozzles. Process Saf. Prog. 24 (1), 29–37. https://doi.org/10.1002/prs.10035.

Downar-Zapolski, P., Bilicki, Z., Bolle, L., Franco, J., 1996. The Non-Equilibrium Relaxation Model for One-Dimensional Flashing Liquid Flow. Int. J. Multiphase Flow 22 (3), 473–483. https://doi.org/10.1016/0301-9322(95)00078-X.

Fauske, H.K., 1985. Flashing Flows or: Some Practical Guidelines for Emergency Release. Plant/Oper. Prog. 4, 132–134. https://doi.org/10.1002/prsb.720040304.

Henry, R.E., "A Study of One- and Two-Component, Two-Phase Flows at Low Qualities", ANL-7430, Argonne National Laboratory (1968).

Henry, R.E., 1970. The Two-Phase Discharge of Initially Saturated or Subcooled Liquid. Nucl. Sci. Eng. 41, 336–342.

Henry, R.E., Fauske, H.K., 1971. The Two-Phase Critical Flow of One-Component Mixtures in Nozzles, Orifices, and Short Tubes. ASME J. Heat Transfer 93, 179–187. https://doi.org/10.1115/1.3449782.

Hodkinson, B., "The Flow of Hot Water through a Nozzle", Engineering, London, 143 (1937), 629–630.

Hsu, Y. Y. "Review of critical flow, propagation of pressure pulse, and sonic velocity", NASA TN D-6814 (1972), https://ntrs.nasa.gov/api/citations/19720019314/downloads/19720019314.pdf.

Kim, Y.-S., 2015a. A proposed correlation for critical flow rate of water flow. Nuclear Eng. Technol. 47 (1), 135–138. https://doi.org/10.1016/j.net.2014.11.004.

Kim, Y.-S., 2015b. Overview of Geometrical Effects on the Critical Flow Rate of Sib-Cooled and Saturated Water. Annals Nucl. Energy 76, 12–18. https://doi.org/10.1016/j.anucene.2014.09.028.

Leung, J.C., "Non-equilibrium Discharge Flow Model for Subcooled, Saturated and Two-Phase Inlet Conditions, DIERS Users Group Meeting, Philadelphia, PA, September 18, 2013.

Leung, J.C., "A Correlation for Subcooled, Saturated and Low-Quality Critical Discharge in Nozzles and Short Tubes", DIERS Users Group Meeting, Burr Ridge, IL, September 16, 2019.

Leung, J.C., Ciolek, W.H., 1994. Flashing Flow Discharge of Initially Subcooled Liquid in Pipes. J. Fluids Eng. 116, 643–645. https://doi.org/10.1115/1.2910325.

Levy, S., Abdollahian, D., 1982. Homogeneous Non-Equilibrium Critical Flow Model. Int. J. Heat Mass Transfer 25 (6), 759–770. https://doi.org/10.1016/0017-9310(82)90088-6.

Lienhard, J.H., Shamsundar, N., Biney, P.O., 1986. Spinodal Lines and Equations of State: A Review. Nucl. Eng. Des. 95, 297–314. https://doi.org/10.1016/0029-5493(86)90056-7.

Marviken Full Scale Critical Flow Tests, Joint Reactor Safety Experiments in the Marviken Power Station Sweden, NUREG/CR-2671 (1982).

Melhem, G., Hendrickson, G., 2020. Quantify Non-Equilibrium Flow and Rapid Phase Transitions. ioMosaic Corporation Technical Paper.

Mengmeng, X., "Thermodynamic and Gas Dynamic Aspects of a BLEVE", PhD Thesis, Delft University of Technology, 2007, doi: http://resolver.tudelft.nl/uuid:a3514a6a-49d8-41b3-ada5-7a7dccb376ea.

Miyatake, O., Tanaka, I., Lior, N., 1997. A Simple Universal Equation for Bubble Growth in Pure Liquids and Binary Solutions with a Non-Volatile Solute. Int. J. Heat Mass Transfer 40 (7), 1577–1584. https://doi.org/10.1016/S0017-9310(96)00224-4.

Moody, F.J., "Maximum Discharge Rate of Liquid-Vapor Mixtures from Vessels", presented in "Non-Equilibrium Two-Phase Flows", ASME Heat Transfer Division Meeting, November 30 – December 5, 1975.

Nilpueng, K., Wongwises, S., 2009. Experimental Investigation of Two-Phase Flow Characteristics of HFC-134a through Short Tube Orifices. Int. J. Refrigeration 32 (5), 854–864. https://doi.org/10.1016/j.ijrefrig.2008.12.003.

Reocreux, M., "Contribution a l'etude des debits critiques en ecoulement diphasique eau-vapor", PhD Thesis, Université Scientifique et Medicale de Grenoble, France (1974), https://babel.hathitrust.org/cgi/pt?id=mdp.39015041730121&view=1up&seq=5.

Saha, P., "Review of Two Phase Steam-Water Critical Flow Models with Emphasis on Thermal Nonequilibrium, NUREG/CR 0417 & BNL-NUREG-50907 (1978).

Sallet, D.W., Somers, G.W., 1985. Flow Capacity and Response of Safety Relief Valves to Saturated Water Flow. Plant / Oper. Prog. 4 (4), 207–216.

Shin, T.S., Jones, O.C., 1993. Nucleation and Flashing in Nozzles – 1. A Distributed Nucleation Model. Int. J. Multiphase Flow 19 (6), 943–964. https://doi.org/10.1016/0301-9322(93)90071-2.

Silver, R., Mitchell, J., 1945. The Discharge of Saturated Water through Nozzles. Trans. North East Coast Inst. Eng. Shipbuilders 62, 51–72.

Schmidt, J., 2007. Sizing of Nozzles, Venturis, Orifices, Control and Safety Valves for Initially Sub-Cooled Gas/Liquid Two-Phase Flow – The HNE-DS MethodAuslegung von Düsen, Venturis, Blenden, Stell- und Sicherheitsventilen für eingangs unterkühlte Gas-Flüssigkeits-Strömungen nach der HNE-DS Methode. Forsch Ingenieurwes 71 (1), 47–58. https://doi.org/10.1007/s10010-006-0043-3.

Seynhaeve, J.-M., De Crécy, A. and Bartosiewicz, Y., "Uncertainty Analysis of Delayed Equilibrium Model (DEM) using the Circle Methodology", NURETH16, Chicago, IL, August 30 – September 4, 2015.

Sozzi, G.L. and Sutherland, W.A., "Critical Flow of Saturated and Subcooled Water at High Pressure", General Electric, NEDO-13418, July 1975.

Sudi, A., Aritomi, M., Murase, A., Iwaki, K., 1994. Relaxation Process of Thermal Non-Equilibrium in Boiling Two-Phase Flow (I). J. Nucl. Sci. Tech 31 (11), 1171–1183. https://doi.org/10.1080/18811248.1994.9735274.

Weisman, J., Tentner, A., 1978. Models for estimation of critical flow in two-phase systems. Prog. Nucl. Energy 2 (3), 183–197. https://doi.org/10.1016/0149-1970(78)90007-0.

Yoon, H.J., Ishii, M., Revankar, S.T., 2006. Choking Flow Modeling with Mechanical and Thermal Non-Equilibrium. Int. J. Heat Mass Transfer 49 (1-2), 171–186. https://doi.org/10.1016/j.ijheatmasstransfer.2005.07.044.